Wave Motion 15 (1992) 229–265
Elsevier

Scalar space-time waves in their spectral-domain first- and second-order Thiele approximations

Maarten V. de Hoop
Koninklijke/Shell Exploratie en Produktie Laboratorium, Volmerlaan 6, 2288 GD Rijswijk, The Netherlands

Adrianus T. de Hoop
Laboratory of Electromagnetic Research, Faculty of Electrical Engineering, Delft University of Technology, P.O. Box 5031, 2600 GA Delft, The Netherlands

Received 31 October 1990, Revised 16 April 1991

For the simple case of the scalar wave motion generated by a point source in an unbounded homogeneous medium, it is investigated what the consequences of the first- and second-order Thiele approximations in the spectral domain are in the space-time domain. To this end, the corresponding spectral domain Green's function is transformed back to the space-time domain with the aid of the modified Cagniard method. The exact solution to the problem is a spherical wave with the same wave shape as the source signature and a single wave front. The first-order Thiele, or parabolic, approximation has a wave front in the shape of a double oblate spheroid, combined with a head-wave-like precursor having a cylindrical wave front. The second-order Thiele approximation contains two wave fronts, one associated with a fast body wave and the other with a slow body wave, in combination with a head-wave-like precursor, the latter again having a cylindrical wave front. From the results, it can be concluded in which regions below or above the source the approximations have sufficient accuracy for application in inversion and "true amplitude" depth migration procedures in geophysical prospecting.

1. Introduction

The first-order Thiele continued-fraction (or parabolic) approximation was introduced in the analysis of wave phenomena by Leontovich and Fock [1]; their field of application was the propagation of electromagnetic waves near the surface of a convex conducting body [2]. Higher-order approximations were considered by Bremmer [3] in the asymptotic evaluation of the integrals that occur in the theory of diffraction of waves by an aperture in a screen. Since then, the parabolic approximation has been applied to various wave problems, amongst which are the propagation of waves in random media [4], the downward continuation of acoustic waves in seismic prospecting [5], and underwater acoustics [6, 7].

In recent years there is an increasing interest in the use of higher-order Thiele-type continued-fraction approximations (which include the parabolic and Padé approximations) in the application of seismic modeling, migration and inversion techniques. We mention the papers by Ristow [8], Ma [9], Lee and Suh [10], Kelamis and Kjartansson [11], and Graves and Clayton [12]. The motivation of the Thiele approximation is the following. For one-dimensional wave propagation it is known that the wave operator can be factorized into two partial differential operators that can be identified as to apply to waves propagating in opposite directions. For wave propagation in more dimensions such a factorization can again be carried out, be it that the factors contain pseudo-differential operators. The latter have no simple discrete counterparts which are sparse in their matrix representation. For a simple and sparse matrix representation of

the desired so-called "one-way" wave operator we need an intermediate partial differential operator. The Thiele approximation, when carried on the slowness in the spectral domain, i.e., after having transformed the actual space-time wave motion to the time Fourier transform (or time Laplace transform) domain and the spatial Fourier transform domain as far as the horizontal coordinates are concerned, about a preferred direction of propagation, yields such a tool. The preferred direction will be identified as the vertical direction. (A Taylor-type approximation leading to such a factorization has been discussed by Corones and Krueger [13].) The resulting partial differential equations, which are denoted as one-way wave equations, are usually solved with the aid of finite-difference techniques carried out in the time Fourier-transform domain [12]. In this respect, it is noted that the stable two-level implicit finite difference integration of a one-way wave equation along the direction of preference leads to a problem of solving a matrix equation. To fully exploit the freedom in the structure of the matrix equation a rational approximation of the vertical slowness as a function of the horizontal slowness is wanted, which is provided by Thiele's formula.

Thiele approximations have been either arrived at with the aid of a perturbation theory applied to the wave equation in a comoving frame of reference [11] or carried out on the wave function in the spectral domain [14, 15]. The properties of the waves in the first-order approximation have, to a certain extent, been studied by Joly [16] and Bamberger et al. [17]; higher-order approximations have been considered by Bamberger et al. [18]. Deviations, due to the approximation, in the phase and group velocities of normal modes in underwater acoustic ducts have been analyzed by McDaniel [6]. Approximations of the vertical slowness were further employed to obtain asymptotic expressions in space-time for the wave constituents associated with the conical points in an anisotropic elastic medium having cubic symmetry [19].

Although the one-way wave equations are strictly valid only in a horizontally homogeneous medium, they have nonetheless been applied in arbitrarily inhomogeneous media. Viewed from this perspective, a Thiele approximation is recognized as a high-frequency approximation that does not suffer from the singularities at which asymptotic ray theory fails (caustics and foci). Proper extensions of the one-way wave equations to fully inhomogeneous media have been discussed by Palmer [20], who also includes a source term in the analysis, and by Fishman and McCoy [21], who employ pseudo-differential operators to account for the mutual coupling between the different spatial Fourier components. A related approach has also been developed by Gazdag [22] and Gazdag and Sguazzero [23].

The Thiele approximants have been compared, in the spectral domain, with approximants of the vertical slowness obtained through least-squares fitting by Lee and Suh [10], through interpolation at a number of values of the horizontal slowness by Halpern and Trefethen [24], and through the replacement of it by an integral representation by Zhang Guan-quan et al. [25].

The relation between the solutions of the exact (Helmholtz) and the first-order approximated (Schrödinger) equations for propagation of sound in an acoustic wave guide has been analyzed by Polyanskii [26] and De Santo [27] to investigate what consequences the approximation of the equation has for the solutions.

The purpose of the present paper is to investigate, for the simple case of the scalar wave motion generated by a point source in an unbounded homogeneous medium, what the consequences of the approximations are in the space-time domain. In this case all calculations can be carried out exactly in closed form. We determine the first- and second-order Thiele approximations of the wave function in the spectral domain and transform the results back to the space-time domain with the aid of the modified Cagniard method as it has been developed by the senior (second) author (cf. [28, 29] and [30, pages 298–301], [31, pages 302–314], [32, pages 243–253] and [33]). (An alternative but equivalent method has been given by Petrowsky [34].) The exact solution to the problem is a spherical wave having the same shape as the source signature and a single wave front. The first-order Thiele approximation turns out to have a composite wave front

consisting of an oblate spheroid associated with the body wave, in combination with a head-wave-like precursor having a cylindrical wave front. The second-order Thiele approximation turns out to have two non-spherical wave fronts associated with two body waves containing cusps, again accompanied by a head-wave-like precursor having a cylindrical wave front. The results enable one to judge in which region of space-time the relevant approximations are accurate enough for use in seismic inversion or migration procedures. In view of these applications, special attention is paid to a comparison with asymptotic ray theory in the vertical direction.

The first- and second-order Thiele approximants are basic in the sense that any odd- or even-order approximation can be written as a summation of terms that resemble the low-order approximants. This implies that the waves associated with the higher-order approximations applied in a homogeneous medium are equivalent to the waves in a quasi-multilayer configuration in which the vertical slowness in each individual layer is given by a first- or second-order-like approximant.

With the aid of Thiele's formula the theory can be extended to anisotropic fluids.

2. The exact wave equation and its solution in the space-time and spectral domains

To locate a point in space we use the coordinates $\{x, x_2, x_3\}$ with respect to the orthogonal Cartesian reference frame with origin $\mathcal{O}$ and the three mutually perpendicular base vectors $\{\mathbf{i}_1, \mathbf{i}_2, \mathbf{i}_3\}$ of unit length each. In the indicated order, the base vectors form a right-handed system. The subscript notation for Cartesian vectors and tensors applies and for repeated subscripts the summation convention holds. Lower-case Latin subscripts are used for this purpose; they are to be assigned the values $\{1, 2, 3\}$. The position vector corresponding to $\{x_1, x_2, x_3\}$ is therefore denoted by $\mathbf{x}=x_m\mathbf{i}_m$. The time coordinate is denoted by t. The symbol ∂_m indicates differentiation with respect to x_m; ∂_t is a reserved symbol for differentiation with respect to time.

The scalar wave function $u=u(\mathbf{x}, t)$ that is representative of the wave motion generated by a point source located at $\{0, 0, 0\}$ and with source signature $f=f(t)$ satisfies the three-dimensional scalar wave equation

$$(\partial_m\partial_m - c^{-2}\partial_t^2)u = -f(t)\delta(x_1, x_2, x_3), \tag{1}$$

where c is the wave speed in the medium and $\delta(x_1, x_2, x_3)$ denotes the three-dimensional unit impulse (Dirac distribution) operative at the point $\{0, 0, 0\}$. The exact solution to this equation is the spherical wave [30]

$$u = f(t-|\mathbf{x}|/c)/4\pi|\mathbf{x}|, \tag{2}$$

where $|\mathbf{x}|=(x_m x_m)^{1/2}$. Its wave shape is the same as the source signature. Equation (2) can also be written as

$$u(\mathbf{x}, t) = \partial_t \int_{t'=|\mathbf{x}|/c}^{t} f(t-t')G(\mathbf{x}, t')\,\mathrm{d}t', \tag{3}$$

where the source is assumed to start acting at the instant $t=0$, and in which

$$G(\mathbf{x}, t)=H(t-|\mathbf{x}|/c)/4\pi|\mathbf{x}|, \tag{4}$$

where $H(t)=\{0, 1/2, 1\}$ for $\{t<0, t=0, t>0\}$ denotes the Heaviside unit step function. Figure 1 shows a snapshot in space of this Green's function.

How the well-known result of eq. (2) can be obtained with the aid of the modified Cagniard method is shown in [28]. For this, as well as for the Thiele approximations of this paper's subsequent sections, the spectral domain representation of u is needed. The latter follows by applying to eq. (1) the one-sided Laplace transformation

$$\hat{u}(\mathbf{x}, s)=\int_{t=0}^{\infty} \exp(-st)u(\mathbf{x}, t)\,\mathrm{d}t, \tag{5}$$

followed by the spatial Fourier transformation with respect to the "horizontal" coordinates x_1 and x_2

$$\tilde{u}(\mathrm{i}\alpha_\mu, x_3, s)=\int_{x_\mu\in\mathscr{R}^2} \exp(\mathrm{i}s\alpha_\mu x_\mu)\hat{u}(x_m, s)\,\mathrm{d}x_1\,\mathrm{d}x_2, \tag{6}$$

where Greek subscripts are used to indicate the horizontal components of vectors and tensors; to them the values $\{1, 2\}$ are to be assigned. In accordance with the Cagniard method, s is chosen to be real and

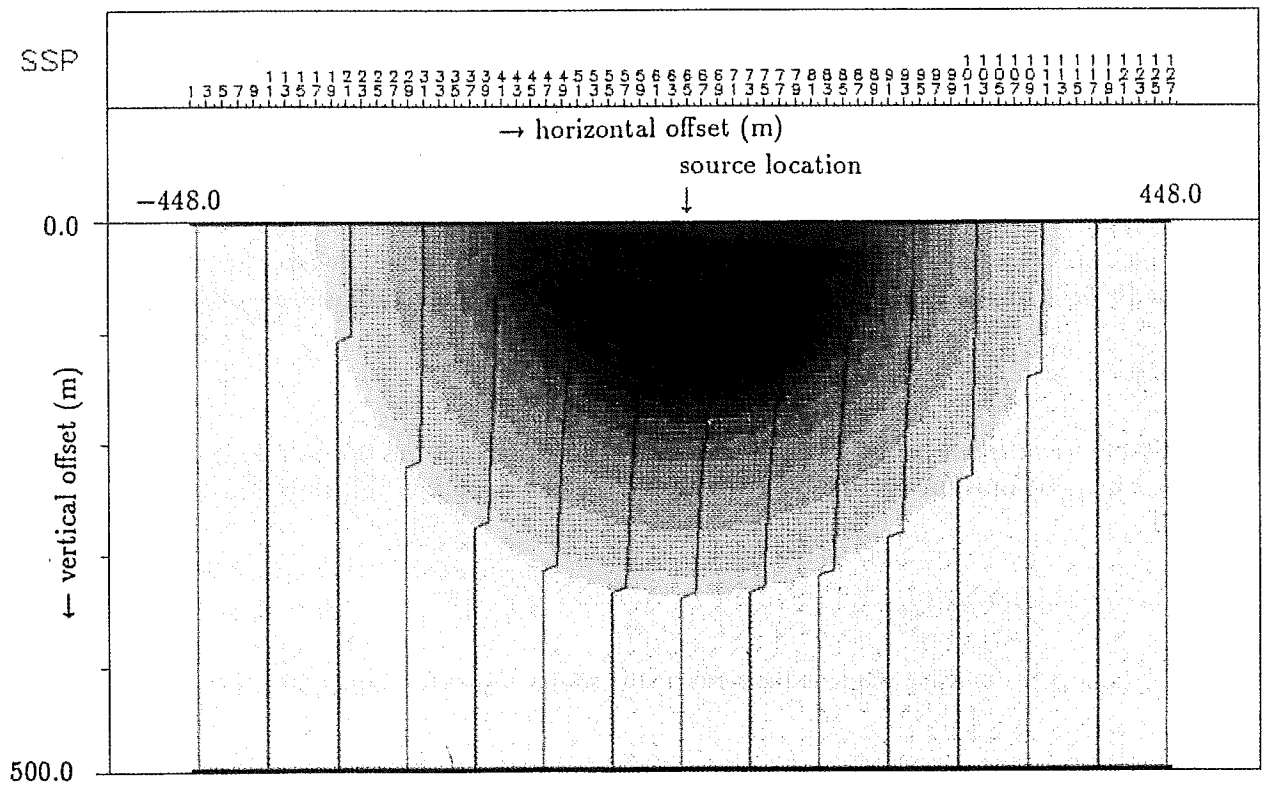

Fig. 1. Snapshot of the exact Green's function in space for $x_3\geqslant 0$; $c=750$ m/s, $t=0.450$ s. (The horizontal offsets are numbered sequentially.)

positive, and α_1 and α_2 are real. The factor s in eq. (6) is introduced for convenience in the transformation back to the space-time domain. The transformation inverse to eq. (6) is given by

$$\hat{u}(x_m, s) = (s/2\pi)^2 \int_{\alpha_\mu \in \mathscr{R}^2} \exp(-is\alpha_\mu x_\mu)\tilde{u}(i\alpha_\mu, x_3, s)\, d\alpha_1\, d\alpha_2. \tag{7}$$

The spectral-domain counterpart $\tilde{u}$ of u then satisfies the ordinary differential equation

$$\partial_3^2\tilde{u} - s^2\gamma^2\tilde{u} = -\hat{f}(s)\delta(x_3), \tag{8}$$

where $\delta(x_3)$ is the one-dimensional unit impulse (Dirac distribution) operative at $x_3 = 0$ and

$$\gamma = (\alpha_\mu\alpha_\mu + c^{-2})^{1/2} > 0 \tag{9}$$

is the spectral-domain "vertical" slowness. The solution of eq. (8) is given by

$$\tilde{u} = \hat{f}(s)\exp(-s\gamma|x_3|)/2s\gamma. \tag{10}$$

To bring eq. (10) into accordance with the form of eq. (3), it is rewritten as

$$\tilde{u} = s\hat{f}(s)\tilde{G}(i\alpha_\mu, x_3, s). \tag{11}$$

Comparing eq. (11) with eq. (10), it is found that

$$\tilde{G} = \exp(-s\gamma|x_3|)/2s^2\gamma. \tag{12}$$

Upon substituting eq. (12) in eq. (7), the algebraic factors of s cancel and only the s in the exponential function remains, which property serves as a criterion for selecting a Green's function in the Cagniard method.

By differentiating the right-hand side of eq. (12) twice with respect to x_3, we can reconstruct the differential equation that $\tilde{G}$ satisfies. In view of the non-analyticity at $x_3 = 0$, this procedure leads to the required volume source density in its right-hand side. Specificially, we obtain

$$\partial_3^2\tilde{G} - s^2\gamma^2\tilde{G} = -s^{-1}\delta(x_3). \tag{13}$$

Now, under the transformations of eqs. (5) and (6), we have $\partial_t \to s$ and $\partial_\mu \to -is\alpha_\mu$. Applying these rules, we reconstruct from eq. (13) the partial differential equation that G satisfies as

$$(\partial_m\partial_m - c^{-2}\partial_t^2)G = -\delta(x_1, x_2, x_3)H(t). \tag{14}$$

Note that the wave operator on the left-hand side does not admit, in three-dimensional space, a factorization into space-time differential operators. (Such a factorization is restricted to only one space dimension.)

3. The first-order Thiele approximation

In the first-order Thiele approximation (see Appendix A), γ in eq. (9) is replaced by

$$\gamma^{\mathrm{I}} = 1/c + (c/2)\alpha_\mu\alpha_\mu. \tag{15}$$

It is noted that this approximation is identical to the first-order Taylor expansion about $c^2\alpha_\mu\alpha_\mu=0$. The resulting spectral-domain wave function is given by

$$\tilde{u}^{\mathrm{I}}=s\hat{f}(s)\tilde{G}^{\mathrm{I}}(\mathrm{i}\alpha_\mu, x_3, s), \tag{16}$$

in which, in view of eq. (12),

$$\tilde{G}^{\mathrm{I}}=\exp(-s\gamma^{\mathrm{I}}|x_3|)/2s^2\gamma^{\mathrm{I}}. \tag{17}$$

To reconstruct the latter's space-time equivalent, we substitute eq. (17) into eq. (7) and apply the modified Cagniard method. This method consists of transforming the variables of integration $\{\alpha_1, \alpha_2\}$ with $\{\alpha_1\in\mathscr{R}, \alpha_2\in\mathscr{R}\}$ into $\{p, q\}$ with $\{p\in\mathscr{I}, q\in\mathscr{R}\}$ (here, $\mathscr{R}$ denotes the real axis and $\mathscr{I}$ the imaginary axis) through

$$\alpha_1=-\mathrm{i}p\cos(\theta)-q\sin(\theta), \tag{18}$$

$$\alpha_2=-\mathrm{i}p\sin(\theta)+q\cos(\theta), \tag{19}$$

where $\{r, \theta\}$ is related to $\{x_1, x_2\}$ by

$$x_1=r\cos(\theta), \qquad x_2=r\sin(\theta), \tag{20}$$

with $0\leqslant r<\infty$, $0\leqslant\theta<2\pi$, keeping q real, continuing the integrand analytically into the complex p-plane and carrying out the integration along the modified Cagniard path that follows from a continuous deformation of the imaginary p-axis satisfying the equation

$$pr+\gamma^{\mathrm{I}}|x_3|=\tau, \tag{21}$$

where τ is real and positive. In view of the condition that the joining paths at infinity must yield a vanishing contribution, contours only in the right half of the complex p-plane are considered. Solving for p in eq. (21), we see that the modified Cagniard path consists of $p=p^{\mathrm{I}}(\tau, q)$ in the first quadrant of the complex p-plane, together with its complex conjugate $p=p^{\mathrm{I}*}(\tau, q)$ in the fourth quadrant of the complex p-plane, where

$$p^{\mathrm{I}}=(r/c|x_3|)+\mathrm{i}(2/c|x_3|)^{1/2}[\tau-T^{\mathrm{I}}(q)]^{1/2} \quad \text{for } T^{\mathrm{I}}(q)\leqslant\tau<\infty, \tag{22}$$

in which

$$T^{\mathrm{I}}(q)=T^{\mathrm{I}}(0)+(c|x_3|/2)q^2, \tag{23}$$

with

$$T^{\mathrm{I}}(0)=(|x_3|/c)(1+r^2/2x_3^2). \tag{24}$$

Equation (22) represents a straight line parallel to the imaginary p-axis that intersects the real p-axis at $p=r/c|x_3|$. Along this path, τ strictly increases when going from the point of intersection with the real p-axis to infinity.

In the process of contour deformation we might possibly encounter the simple pole $p=p_0^{\mathrm{I}}$ of $\tilde{G}^{\mathrm{I}}$ at the simple zero of γ^{I} in the right half of the p-plane (cf. eq. (17)). From eqs. (15), (18) and (19) it follows that

$$p_0^{\mathrm{I}}=(q^2+2/c^2)^{1/2}>0. \tag{25}$$

This pole contributes to the Green's function when it lies to the left of the point of intersection of the modified Cagniard path with the real p-axis. In the case where $r<|x_3|\sqrt{2}$ ("small" horizontal offset), the

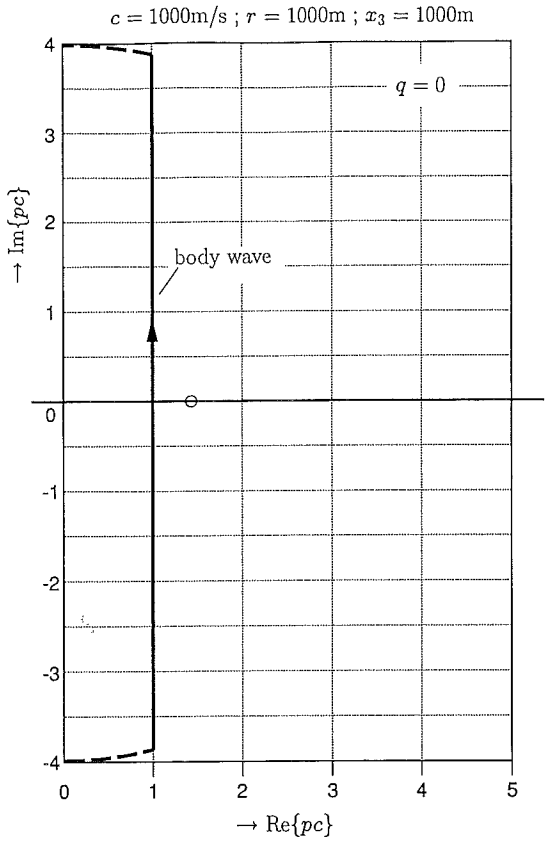

Fig. 2. The modified Cagniard contour and the pole location for a "small" horizontal offset in the first-order Thiele approximation.

simple pole lies, for all values of q, to the right of the point of intersection of the modified Cagniard path with the real p-axis and is not passed in the process of contour deformation (see Fig. 2).

3.1. *The body wave*

In the integral along the modified Cagniard path, τ is introduced as the variable of integration. The corresponding one-dimensional Jacobian follows from Eq. (22) as

$$\partial p^{\mathrm{I}}/\partial\tau = \mathrm{i}(2c|x_3|)^{-1/2}[\tau - T^{\mathrm{I}}(q)]^{-1/2}. \tag{26}$$

Taking the contributions from $p=p^{\mathrm{I}}$ and $p=p^{\mathrm{I}*}$ together (note that the integrand satisfies Schwarz's reflection principle), the contribution from the Cagniard path is arrived at through eq. (7):

$$\hat{u}^{\mathrm{I}}_{\mathrm{C}}(x_m, s) = s\hat{f}(s)\hat{G}^{\mathrm{I}}_{\mathrm{C}}(x_m, s), \tag{27}$$

in which

$$\hat{G}^{\mathrm{I}}_{\mathrm{C}} = \pi^{-2}\,\mathrm{Im}\left\{\int_{q=0}^{\infty} \mathrm{d}q \int_{\tau=T^{\mathrm{I}}(q)}^{\infty} \exp(-s\tau)[2\gamma^{\mathrm{I}}(p^{\mathrm{I}}, q)]^{-1}(\partial p^{\mathrm{I}}/\partial\tau)\,\mathrm{d}\tau\right\}. \tag{28}$$

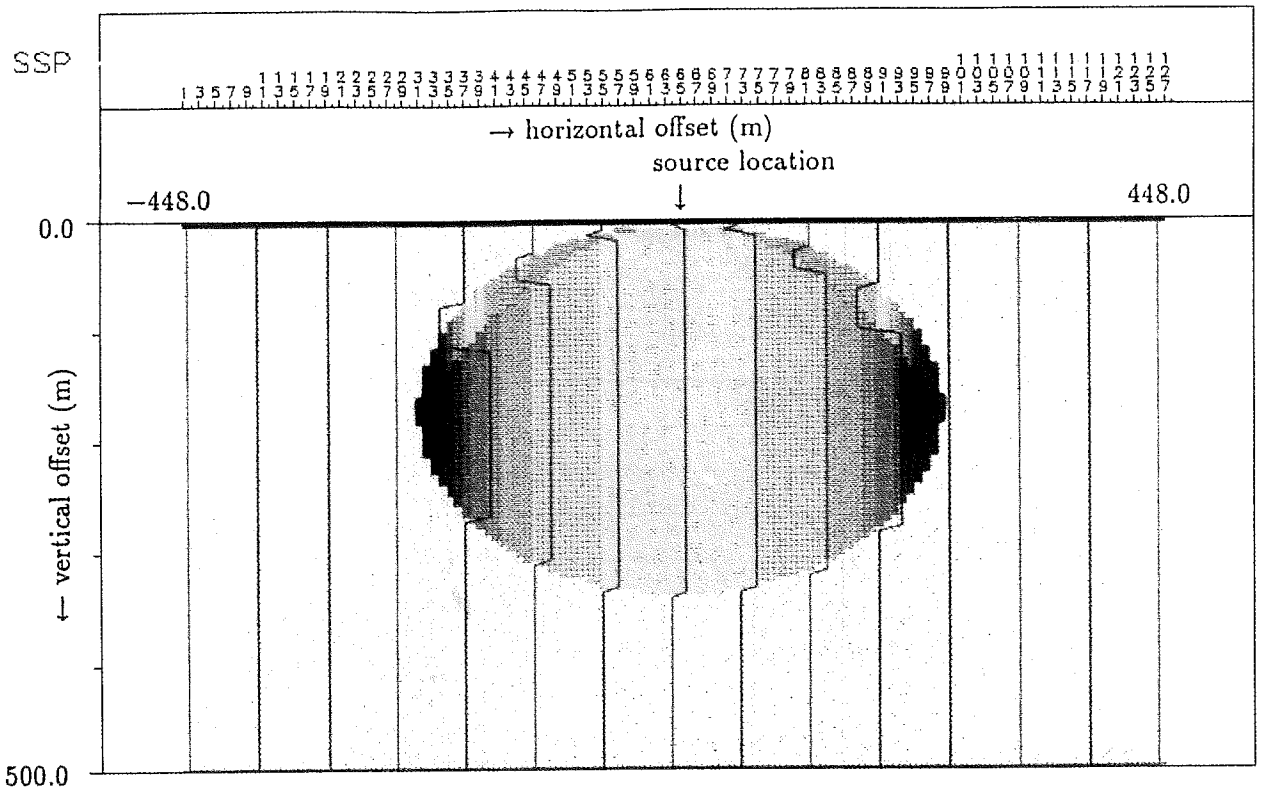

Fig. 3. Snapshot of the Cagniard-path contribution to the Green's function in space for $x_3 \geqslant 0$ in the first-order Thiele approximation; $c = 750$ m/s, $t = 0.450$ s. (The horizontal offsets are numbered sequentially.)

Interchanging the order of integration yields

$$\hat{G}^{\mathrm{I}}_{\mathrm{C}} = \int_{\tau = T^{\mathrm{I}}(0)}^{\infty} \exp(-s\tau)\, \mathrm{d}\tau \int_{q=0}^{Q^{\mathrm{I}}(\tau)} \pi^{-2}\, \mathrm{Im}\{[2\gamma^{\mathrm{I}}(p^{\mathrm{I}}, q)]^{-1}(\partial p^{\mathrm{I}}/\partial \tau)\}\, \mathrm{d}q, \tag{29}$$

in which $q = Q^{\mathrm{I}}(\tau)$, the (unique) inverse of $\tau = T^{\mathrm{I}}(q)$, is given by

$$Q^{\mathrm{I}}(\tau) = (2/c|x_3|)^{1/2}[\tau - T^{\mathrm{I}}(0)]^{1/2}. \tag{30}$$

Application of Lerch's theorem on the uniqueness of the Laplace transform of a causal time function when taken at positive real values of s [35, pages 61–63] leads to the time-domain results

$$G^{\mathrm{I}}_{\mathrm{C}} = \left[\int_{q=0}^{Q^{\mathrm{I}}(t)} \pi^{-2}\, \mathrm{Im}\{[2\gamma^{\mathrm{I}}(p^{\mathrm{I}}, q)]^{-1}(\partial p^{\mathrm{I}}/\partial \tau)\}\, \mathrm{d}q\right] H[t - T^{\mathrm{I}}(0)] \tag{31}$$

and

$$u^{\mathrm{I}}_{\mathrm{C}}(x_m, t) = \partial_t \int_{t' = T^{\mathrm{I}}(0)}^{t} f(t - t') G^{\mathrm{I}}_{\mathrm{C}}(x_m, t')\, \mathrm{d}t', \tag{32}$$

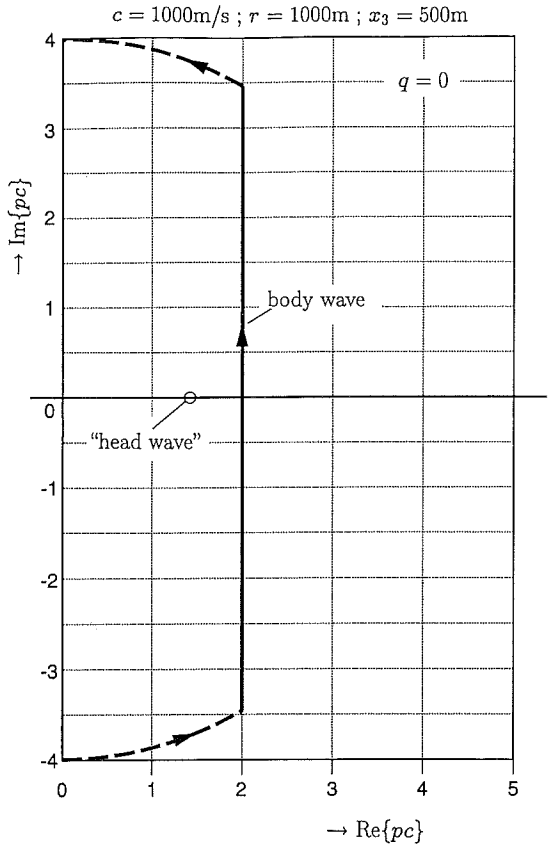

Fig. 4. The modified Cagniard contour and the pole location for a "large" horizontal offset in the first-order Thiele approximation.

from which it is evident that $T^{\mathrm{I}}(0)$, as given by eq. (24), is the arrival time of the wave. The equation for the corresponding wave front follows from eq. (24) as

$$[|x_3|-cT^{\mathrm{I}}(0)/2]^2+r^2/2=[cT^{\mathrm{I}}(0)/2]^2, \tag{33}$$

which is a double oblate spheroid centered on $r=0$ and $|x_3|=cT^{\mathrm{I}}(0)/2$ with semiminor axis $cT^{\mathrm{I}}(0)/2$ and semimajor axis $cT^{\mathrm{I}}(0)/\sqrt{2}$. Through the substitution

$$q=Q^{\mathrm{I}}(t)\sin(\psi), \tag{34}$$

the integral in eq. (31) can be evaluated in closed form. The result is

$$G^{\mathrm{I}}_{\mathrm{C}}=\frac{1}{4\pi c(t^2-2r^2/c^2)^{1/2}}\,\mathrm{sgn}(t-r^2/c|x_3|)H[t-T^{\mathrm{I}}(0)]. \tag{35}$$

Figure 3 shows a snapshot in space of this Green's function for $x_3\geqslant 0$.

3.2. The precursor

When $r>|x_3|\sqrt{2}$ ("large" horizontal offset), the simple pole p^{I}_0 lies to the left of the point of intersection of the modified Cagniard path with the real p-axis if $q^2<(q^{\mathrm{I}}_0)^2$, where $q^{\mathrm{I}}_0=[(r/c|x_3|)^2-2/c^2]^{1/2}$. In this case,

the pole's contribution has to be taken into account in the process of contour deformation, as illustrated in Fig. 4. The relevant contribution is found to be

$$\hat{G}_0^{\mathrm{I}}=\frac{1}{2\pi c}\int_{q=0}^{q_0^{\mathrm{I}}}\frac{\exp[-sr(q^2+2/c^2)^{1/2}]}{(q^2+2/c^2)^{1/2}}\,\mathrm{d}q, \tag{36}$$

which, upon replacing $r(q^2+2/c^2)^{1/2}$ by τ, takes the form

$$\hat{G}_0^{\mathrm{I}}=\frac{1}{2\pi c}\int_{\tau=T_{0,1}^{\mathrm{I}}}^{T_{0,2}^{\mathrm{I}}}\frac{\exp(-s\tau)}{(\tau^2-2r^2/c^2)^{1/2}}\,\mathrm{d}\tau, \tag{37}$$

in which

$$T_{0,1}^{\mathrm{I}}=\sqrt{2}(r/c)\quad\text{and}\quad T_{0,2}^{\mathrm{I}}=(r/|x_3|)(r/c). \tag{38}$$

On account of Lerch's theorem on the uniqueness of the Laplace transform of a causal time function when taken at positive real values of s, the time domain counterpart G_0^{I} of $\hat{G}_0^{\mathrm{I}}$ then follows as

$$G_0^{\mathrm{I}}=\frac{1}{2\pi c[t^2-(T_{0,1}^{\mathrm{I}})^2]^{1/2}}[H(t-T_{0,1}^{\mathrm{I}})-H(t-T_{0,2}^{\mathrm{I}})]. \tag{39}$$

This contribution (see Fig. 5), which is present only if $r>|x_3|\sqrt{2}$, is to be added to the contribution from

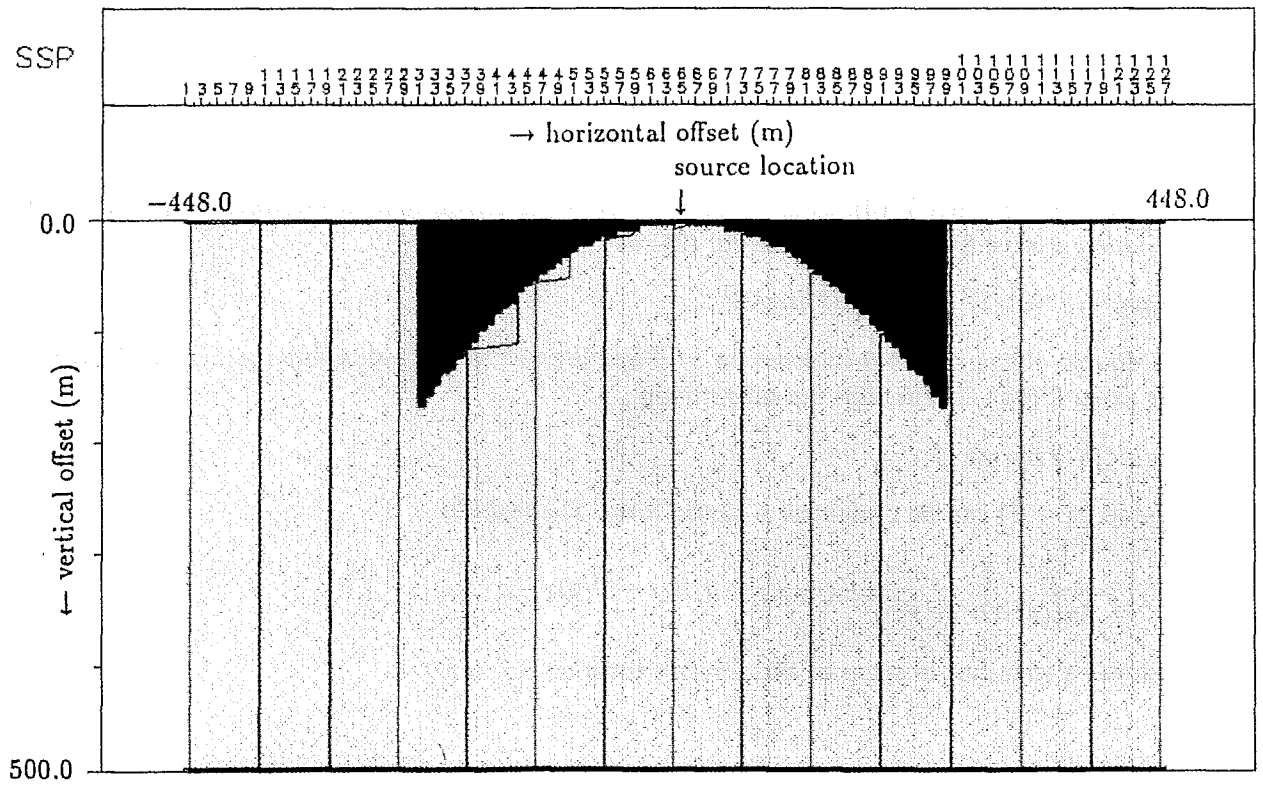

Fig. 5. Snapshot of the pole contribution to the Green's function in space for $x_3\geqslant 0$ in the first-order Thiele approximation; $c=$ 750 m/s, $t=0.450$ s. (The horizontal offsets are numbered sequentially.)

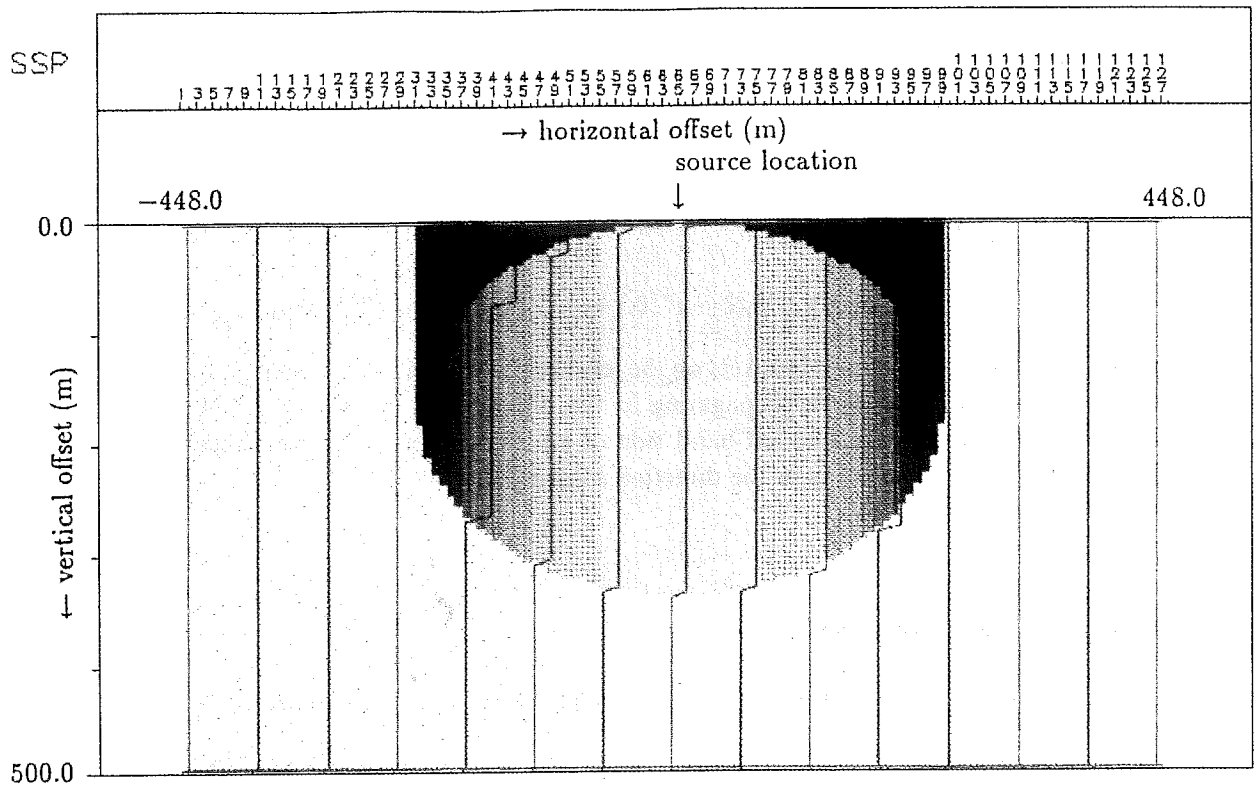

Fig. 6. Snapshot of the total Green's function in space for $x_3 \geqslant 0$ in the first-order Thiele approximation; $c=750$ m/s, $t=0.450$ s. (The horizontal offsets are numbered sequentially.)

the modified Cagniard path eq. (35). The corresponding wave front has a cylindrical shape and touches the spheroid of G_C^I. It can be interpreted as a head-wave-like precursor. Figure 6 shows a snapshot in space of the total Green's function $G_C^I + G_0^I$ for $x_3 \geqslant 0$.

3.3. *The case* $x_3 = 0$

In the case $x_3 = 0$, the expression in eq. (22) breaks down; from eq. (21) it follows that the modified Cagniard contour coincides with the real, positive p-axis. In view of the analyticity of the integrand away from the pole, the expression for $\hat{G}^I$ reduces to the contribution from the pole only, i.e., (cf. eq. (36))

$$\hat{G}_0^I = \frac{1}{2\pi c} \int_{q=0}^{\infty} \frac{\exp[-sr(q^2 + 2/c^2)^{1/2}]}{(q^2 + 2/c^2)^{1/2}} \, dq. \tag{40}$$

The space-time counterpart to this expression is found to be (cf. eq. (39))

$$G_0^I = \frac{1}{2\pi c[t^2 - (T_{0,1}^I)^2]^{1/2}} H(t - T_{0,1}^I), \tag{41}$$

in which $T_{0,1}^I$ is given by eq. (38).

3.4. *Partial differential equation for* G^{I}

By differentiating the right-hand side of eq. (17) twice with respect to x_3, and using that under the transformations of eqs. (5) and (6) we have $\partial_t \to s$ and $\partial_\mu \to -is\alpha_\mu$, we can reconstruct the partial differential equation that G^{I} satisfies, viz.,

$$c^{-2}\partial_t^2(\partial_m\partial_m - c^{-2}\partial_t^2)G^{\mathrm{I}} - (1/4)(\partial_\mu\partial_\mu)^2 G^{\mathrm{I}} = -c^{-2}\partial_t^2\delta(x_1, x_2, x_3)H(t). \tag{42}$$

This equation factorizes as

$$[c^{-1}\partial_t(\partial_3 + c^{-1}\partial_t) - (1/2)\partial_\mu\partial_\mu][c^{-1}\partial_t(\partial_3 - c^{-1}\partial_t) + (1/2)\partial_\nu\partial_\nu]G^{\mathrm{I}} = -c^{-2}\partial_t^2\delta(x_1, x_2, x_3)H(t). \tag{43}$$

The first partial differential operator in brackets on the left-hand side of eq. (43) is the parabolic approximation to the wave operator for a wave propagating in the direction of increasing x_3; the second partial differential operator in brackets on the left-hand side of eq. (43) is the parabolic approximation to the wave operator for a wave propagating in the direction of decreasing x_3 [5].

4. The second-order Thiele approximation

In the second-order Thiele approximation (see Appendix A), γ in eq. (9) is replaced by

$$\gamma^{\mathrm{II}} = \frac{3}{c}\frac{4/3c^2 + \alpha_\mu\alpha_\mu}{4/c^2 + \alpha_\nu\alpha_\nu}. \tag{44}$$

The resulting spectral-domain wave function is given by

$$\tilde{u}^{\mathrm{II}} = s\hat{f}(s)\tilde{G}^{\mathrm{II}}(i\alpha_\mu, x_3, s), \tag{45}$$

in which

$$\tilde{G}^{\mathrm{II}} = \exp(-s\gamma^{\mathrm{II}}|x_3|)/2s^2\gamma^{\mathrm{II}}. \tag{46}$$

To reconstruct the latter's space-time equivalent, we substitute eq. (46) into eq. (7) and apply the modified Cagniard method. First, however, it should be noted that upon replacing γ in eq. (9) by γ^{II} according to eq. (44), the inversion integral eq. (7) becomes divergent, since $\gamma^{\mathrm{II}} \to 3/c$ as $\alpha_\mu\alpha_\mu \to \infty$. A physically meaningful interpretation of the integral must therefore be found. The asymptotic structure of the integrand eq. (45) as $\alpha_\mu\alpha_\mu \to \infty$ leads to the conjecture that the divergent integral contains a contribution that could be interpreted as a Dirac delta distribution operative at $\{x_1 = 0, x_2 = 0\}$. In view of this conjecture and of the contour deformation to follow, it is assumed that an interpretation in the sense of a Cauchy principal value around infinity will lead to a physically acceptable result. Adopting this interpretation, the integral on the right-hand side of eq. (7) is replaced by the limit of the integral over the rectangle $\{\alpha_1 \in \mathscr{R},\ \alpha_2 \in \mathscr{R};\ -\Delta_{\alpha_1} < \alpha_1 < \Delta_{\alpha_1},\ -\Delta_{\alpha_2} < \alpha_2 < \Delta_{\alpha_2}\}$ with $\Delta_{\alpha_1} \to \infty$ and $\Delta_{\alpha_2} \to \infty$. The corresponding evaluation will be carried out later in this paper.

The modified Cagniard method consists of applying the transformation given by eqs. (18) and (19), in which q is kept real. The resulting integral with respect to p is extended over $\{p \in \mathscr{I};\ -\mathrm{i}\Delta < p < \mathrm{i}\Delta\}$ with $\Delta \to \infty$. The integrand is continued analytically into the complex p-plane and an integration is carried out

along the modified Cagniard path that follows from a continuous deformation of the imaginary p-axis satisfying the equation

$$pr+|x_3|\gamma^{\mathrm{II}}=\tau, \tag{47}$$

where τ is real and positive. The expression for γ^{II} is written as

$$\gamma^{\mathrm{II}}=\frac{3}{c}\left[1-\frac{A^2}{B^2(q)-p^2}\right], \tag{48}$$

with

$$A^2=8/3c^2, \tag{49}$$

$$B^2(q)=4/c^2+q^2. \tag{50}$$

The non-real-axis part of the solution of the cubic equation (47) along which τ strictly increases, is the desired modified Cagniard path. In view of the condition that the joining circular arcs at infinity must, after compensation for the principal value around infinity, yield a vanishing contribution, contours only in the right half of the complex p-plane are considered. The desired contour consists of $p=p^{\mathrm{II}}(\tau, q)$ in the first quadrant of the complex p-plane, together with its complex conjugate $p=p^{\mathrm{II}*}(\tau, q)$ in the fourth quadrant of the complex p-plane. Its explicit form is obtained from Cardano's formula for the solution of the algebraic cubic equation; the relevant expression is given in Appendix B. For the moment we only need a number of properties that can directly be obtained from eq. (47).

The first is that $p=p^{\mathrm{II}}(\tau, q)$ and $p=p^{\mathrm{II}*}(\tau, q)$ are finite arcs that leave the real p-axis at $p_1^{\mathrm{II}}(q)$, at which point the value of τ is denoted by $T_1^{\mathrm{II}}(q)$, and return to the real p-axis again at $p_2^{\mathrm{II}}(q)$, at which point the value of τ is denoted by $T_2^{\mathrm{II}}(q)$. Since both arcs leave the real p-axis at the same point and return again to the real p-axis at the same points, these points are double roots of the cubic equation (47). Consequently, $\partial\tau/\partial p=0$ at these points. By differentiating eq. (47) with repect to p, this condition can be expressed as

$$\frac{\partial\tau}{\partial p}=r-\frac{3|x_3|}{c}\frac{2pA^2}{[B^2(q)-p^2]^2}=0 \quad \text{at } p=p_1^{\mathrm{II}}(q) \text{ and } p=p_2^{\mathrm{II}}(q). \tag{51}$$

Inspection of the behavior of τ as a function of p along the real p-axis reveals that $p_1^{\mathrm{II}}(q)<B(q)$ and $p_2^{\mathrm{II}}(q)>B(q)$, which implies that (cf. eq. (47))

$$T_1^{\mathrm{II}}(q)<B(q)r+3|x_3|/c \quad \text{for all } q \tag{52}$$

and

$$T_2^{\mathrm{II}}(q)\geqslant B(q)r+3|x_3|/c \quad \text{for all } q. \tag{53}$$

The equality in the latter equation occurs in the exceptional case that $r=0$, which will be discussed below. It follows that $T_1^{\mathrm{II}}(q)<T_2^{\mathrm{II}}(q)$ for all q, as shown in Fig. 7.

The second property is that along the arcs $p=p^{\mathrm{II}}(\tau, q)$ and $p=p^{\mathrm{II}*}(\tau, q)$, τ strictly increases. This is proved by a *reductio ad absurdum*. Differentiation of eq. (51) with respect to p leads to

$$\frac{\partial^2\tau}{\partial p^2}=-\frac{6|x_3|}{c}\frac{A^2[B^2(q)+3p^2]}{[B^2(q)-p^2]^3}, \tag{54}$$

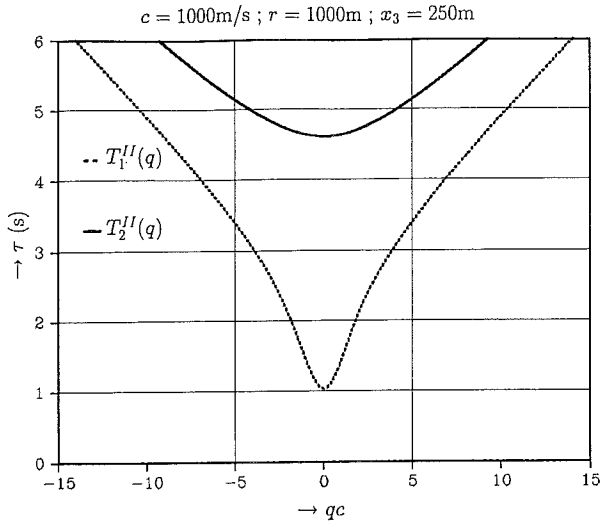

Fig. 7. The $T^{II}_{1,2}$ vs. q-relations; the area between the curves is the domain of integration.

from which it follows that

$$\partial^2\tau/\partial p^2<0 \quad \text{at } p=p_1^{II}(q) \tag{55}$$

and

$$\partial^2\tau/\partial p^2>0 \quad \text{at } p=p_2^{II}(q). \tag{56}$$

Considering the local Taylor expansions about $p=p_1^{II}(q)$ and $p=p_2^{II}(q)$, it then follows that along $p=p^{II}(\tau, q)$ and $p=p^{II*}(\tau, q)$, τ increases away from $p_1^{II}(q)$ and towards $p_2^{II}(q)$. Now, if somewhere on the arc $p=p^{II}(\tau, q)$ there were other points at which $\partial\tau/\partial p=0$, these points must be even in number with a minimum of two, while on the arc $p=p^{II*}(\tau, q)$ there would have to be the same number of such points. This would imply that the quartic equation (51) in p would have at least six solutions, which is impossible. Hence, along the modified Cagniard paths no zeros of $\partial\tau/\partial p$ occur and τ strictly increases. In the limit $|x_3|\downarrow 0$ and $r\neq 0$, Eq. (51) implies that both points of intersection, $p_1^{II}(q)$ and $p_2^{II}(q)$, approach the value $B(q)$. The modified Cagniard contour then contracts to the point $p(\tau, q)=B(q)$. Since, according to eq. (47), in this limit $\tau=pr$ is real, we have

$$T^{II}_{1,2}(q)=B(q)r, \tag{57}$$

which explains the equality sign in eq. (53). Finally, differentiation of eq. (47) with respect to q yields

$$\frac{\partial\tau}{\partial q}=\frac{3|x_3|}{c}\frac{2qA^2}{[B^2(q)-p^2]^2}, \tag{58}$$

from which it follows that at $p=p_1^{II}(q)$ and $p=p_1^{II}(q)$

$$\partial T_1^{II}(q)/\partial q>0 \quad \text{and} \quad \partial T_2^{II}(q)/\partial q>0 \quad \text{for all } q>0, \tag{59}$$

while $q=0$ is a minimum of both $\tau=T_1^{\mathrm{II}}(q)$ and $\tau=T_2^{\mathrm{II}}(q)$. To arrive at an equation for $\tau=T^{\mathrm{II}}(q)$, we eliminate p from eqs. (47) and (51). To this end, eq. (48) is substituted into eq. (47), which leads to

$$(B^2(q)-p^2)(pr+\zeta-\tau)-\zeta A^2=0, \tag{60}$$

where $\zeta=3|x_3|/c$. Differentiating the latter equation with respect to p and substituting the condition for double roots of eq. (47), i.e., $\partial_p\tau=0$, yields

$$p^2-2p\frac{\tau-\zeta}{3r}-\frac{B^2(q)}{3}=0, \tag{61}$$

which equation is equivalent to eq. (51). From eq. (61) an expression for $p^2-B^2(q)$ is obtained, which is substituted into eq. (60). In this way, it follows that

$$p^2-2p\left[\frac{B^2(q)r}{2(\tau-\zeta)}+\frac{\tau-\zeta}{2r}\right]+B^2(q)+\frac{3\zeta A^2}{2(\tau-\zeta)}=0. \tag{62}$$

It is observed that eqs. (61) and (62) are equivalent to eqs. (60) and (61). Using the fact that the roots of eqs. (61) and (62) must coincide, a systematic elimination of the square-root expressions in the resulting equality leads to the final equation:

$$\left[\frac{4}{3}B^2(q)+\frac{3\zeta A^2}{2(T^{\mathrm{II}}(q)-\zeta)}\right]^2-4\left[\frac{B^4(q)r}{6(T^{\mathrm{II}}(q)-\zeta)}+\frac{B^2(q)(T^{\mathrm{II}}(q)-\zeta)}{2r}+\frac{\zeta A^2}{2r}\right]$$

$$\times\left[\frac{T^{\mathrm{II}}(q)-\zeta}{6r}+\frac{B^2(q)r}{2(T^{\mathrm{II}}(q)-\zeta)}\right]=0, \tag{63}$$

where we have set $\tau=T^{\mathrm{II}}(q)$. This equation is equivalent to eq. (B.7) in Appendix B. By setting $q=0$, and substituting ζ, a quartic equation for the arrival times, i.e., the minima $T_{1,2}^{\mathrm{II}}(0)$ of $T_{1,2}^{\mathrm{II}}(q)$, is obtained:

$$T^{\mathrm{II}}(0)^4-10\left(\frac{|x_3|}{c}\right)T^{\mathrm{II}}(0)^3+4\left[9\left(\frac{|x_3|}{c}\right)^2-2\left(\frac{r}{c}\right)^2\right]T^{\mathrm{II}}(0)^2-6\left(\frac{|x_3|}{c}\right)\left[9\left(\frac{|x_3|}{c}\right)^2+4\left(\frac{r}{c}\right)^2\right]T^{\mathrm{II}}(0)$$

$$+27\left(\frac{|x_3|}{c}\right)^4+36\left(\frac{|x_3|}{c}\right)^2\left(\frac{r}{c}\right)^2+16\left(\frac{r}{c}\right)^4=0. \tag{64}$$

Now that the properties of the modified Cagniard path $\{p=p^{\mathrm{II}}(\tau,q)\cup p=p^{\mathrm{II}*}(\tau,q)\}$ have been investigated, the contour deformation leading from the integration along the imaginary p-axis to the one along the modified Cagniard path is further analyzed.

4.1. The body waves

In view of Cauchy's theorem the integral along the imaginary p-axis is equal to the sum of the integrals along the semicircle $\mathscr{C}_\Delta^+=\{p\in\mathscr{C};\,|p|=\Delta,\,\mathrm{Re}(p)>0\}$ and the modified Cagniard path (Fig. 8). In addition,

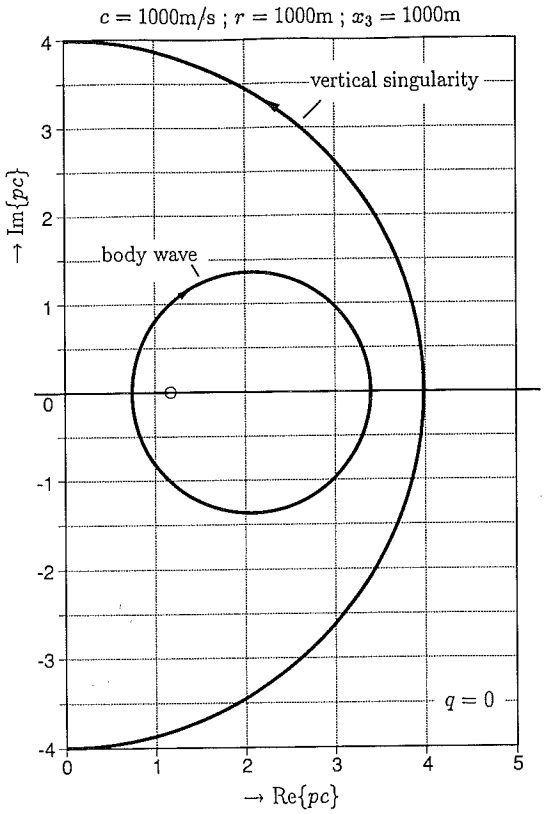

Fig. 8. The modified Cagniard contour and the pole location for a "small" horizontal offset in the second-order Thiele approximation.

we may encounter the simple pole $p=p_0^{\mathrm{II}}$ of $\tilde{G}^{\mathrm{II}}$ at the simple zero of γ^{II} (Fig. 9). From eq. (48) it follows that

$$p_0^{\mathrm{II}}=(q^2+4/3c^2)^{1/2}<B(q) \quad \text{for all } q \tag{65}$$

(cf. eq. (50)). The pole contributes to the Green's function when $p_0^{\mathrm{II}}\leqslant p_1^{\mathrm{II}}$; its contribution will be determined later on. (Since $p_2^{\mathrm{II}}(q)>B(q)$, the situation $p_0^{\mathrm{II}}>p_2^{\mathrm{II}}$ can never arise.) On $\mathscr{C}_\Delta^+$, $\tilde{G}^{\mathrm{II}}$ is asymptotically equal to $(c/6s^2)\exp(-3s|x_3|/c)$. Using the corresponding asymptotic integrand, and carrying out the transformation inverse to eqs. (18) and (19), it follows that the contribution of $\mathscr{C}_\Delta^+$ results into

$$\lim_{\Delta_{\alpha_1}\to\infty,\Delta_{\alpha_2}\to\infty}(s/2\pi)^2\int_{\alpha_1=-\Delta_{\alpha_1}}^{\Delta_{\alpha_1}}\mathrm{d}\alpha_1\int_{\alpha_2=-\Delta_{\alpha_2}}^{\Delta_{\alpha_2}}\exp(-\mathrm{i}s\alpha_\mu x_\mu)(c/6s^2)\exp(-3s|x_3|/c)\,\mathrm{d}\alpha_2$$

$$=(c/6s^2)\exp(-3s|x_3|/c)\delta(x_1,x_2). \tag{66}$$

Furthermore, by taking the contributions from $p=p^{\mathrm{II}}(\tau,q)$ and $p=p^{\mathrm{II}*}(\tau,q)$ together (note that the integrand satisfies Schwarz's reflection principle), the contour part $\hat{G}_{\mathrm{C}}^{\mathrm{II}}$ of the expression for $\hat{G}^{\mathrm{II}}$ is

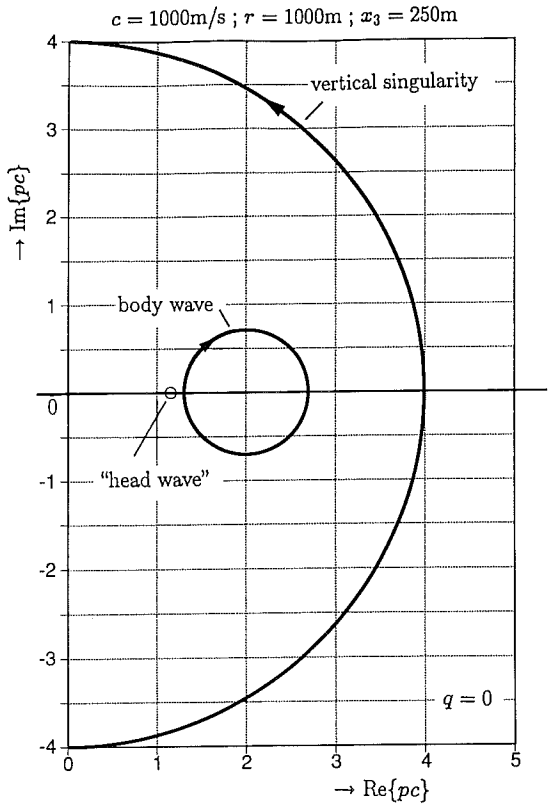

Fig. 9. The modified Cagniard contour and the pole location for a "large" horizontal offset in the second-order Thiele approximation.

obtained

$$\hat{G}_C^{II} = (c/6s^2)\exp(-3s|x_3|/c)\delta(x_1, x_2) + \pi^{-2}\,\mathrm{Im}\left\{\int_{q=0}^{\infty} \mathrm{d}q \int_{\tau=T_1^{II}(q)}^{T_2^{II}(q)} \exp(-s\tau)[2\gamma^{II}(p^{II}, q)]^{-1}(\partial p^{II}/\partial\tau)\,\mathrm{d}\tau\right\}, \tag{67}$$

where also the property has been used that the integrand is an even function of q. Interchanging the order of integration yields (see Fig. 7)

$$\begin{aligned}\hat{G}_C^{II} = {} & (c/6s^2)\exp(-3s|x_3|/c)\delta(x_1, x_2) \\ & + \int_{\tau=T_1^{II}(0)}^{T_2^{II}(0)} \exp(-s\tau)\,\mathrm{d}\tau \int_{q=0}^{Q_1^{II}(\tau)} \pi^{-2}\,\mathrm{Im}\{[2\gamma^{II}(p^{II}, q)]^{-1}(\partial p^{II}/\partial\tau)\,\mathrm{d}q\} \\ & + \int_{\tau=T_2^{II}(0)}^{\infty} \exp(-s\tau)\,\mathrm{d}\tau \int_{q=Q_2^{II}(\tau)}^{Q_1^{II}(\tau)} \pi^{-2}\,\mathrm{Im}\{[2\gamma^{II}(p^{II}, q)]^{-1}(\partial p^{II}/\partial\tau)\,\mathrm{d}q\},\end{aligned} \tag{68}$$

in which $q=Q_1^{\mathrm{II}}(\tau)$ and $q=Q_2^{\mathrm{II}}(\tau)$ are respectively the (unique) inverses of $\tau=T_1^{\mathrm{II}}(q)$ and $\tau=T_2^{\mathrm{II}}(q)$. As eq. (63) shows, these inverses follow from a cubic equation in q^2. Application of Lerch's theorem on the uniqueness of the Laplace transform of a causal time function, taken at positive real values of s, leads to the time-domain results

$$G_C^{\mathrm{II}}=(c/6)(t-3|x_3|/c)H(t-3|x_3|/c)\delta(x_1,x_2)$$
$$+\left[\int_{q=0}^{Q_1^{\mathrm{II}}(t)}\pi^{-2}\,\mathrm{Im}\{[2\gamma^{\mathrm{II}}(p^{\mathrm{II}},q)]^{-1}(\partial p^{\mathrm{II}}/\partial\tau)\}\,\mathrm{d}q\right]\{H[t-T_1^{\mathrm{II}}(0)]-H[t-T_2^{\mathrm{II}}(0)]\}$$
$$+\left[\int_{q=Q_2^{\mathrm{II}}(t)}^{Q_1^{\mathrm{II}}(t)}\pi^{-2}\,\mathrm{Im}\{[2\gamma^{\mathrm{II}}(p^{\mathrm{II}},q)]^{-1}(\partial p^{\mathrm{II}}/\partial\tau)\}\,\mathrm{d}q\right]H[t-T_2^{\mathrm{II}}(0)] \tag{69}$$

and

$$u_C^{\mathrm{II}}(x_m,t)=\partial_t\int_{t'=0}^{t}f(t-t')G_C^{\mathrm{II}}(x_m,t-t')\,\mathrm{d}t', \tag{70}$$

from which it is evident that $t=T_1^{\mathrm{II}}(0)$ and $t=T_2^{\mathrm{II}}(0)$ are the arrival times of the two wave fronts. Through the substitution

$$q=Q_1^{\mathrm{II}}(t)\sin(\psi)\quad\text{with } 0\leqslant\psi\leqslant\pi/2, \tag{71}$$

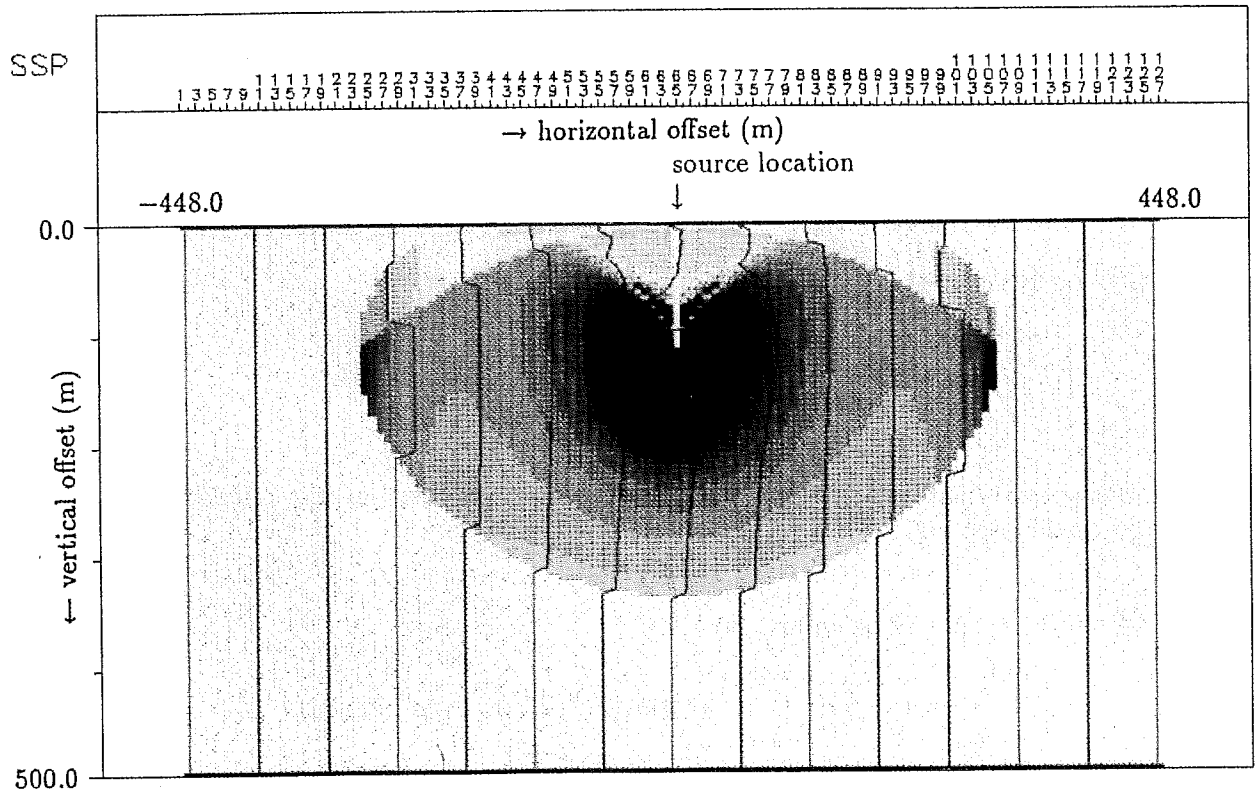

Fig. 10. Snapshot of the Cagniard-path contribution to the Green's function in space for $x_3\geqslant 0$ in the second-order Thiele approximation; $c=750$ m/s, $t=0.450$ s. (The horizontal offsets are numbered sequentially.)

the inverse-square-root singularity at the upper limit of the first integral on the right-hand side of eq. (69) is removed, while through the substitution

$$q=\{[Q_2^{\mathrm{II}}(t)]^2\cos^2(\psi)+[Q_1^{\mathrm{II}}(t)]^2\sin^2(\psi)\}^{1/2} \quad \text{with } 0\leqslant\psi\leqslant\pi/2, \tag{72}$$

the inverse-square-root singularities at both limits of the second integral in eq. (69) are removed. After these substitutions, the integrals are evaluated numerically with the aid of the trapezoidal rule. Figure 10 shows the result in the form of a snapshot in space for $x_3\geqslant 0$. The wave with the arrival time $T_1^{\mathrm{II}}(0)$ will be denoted as the fast body wave; the wave wth the arrival time $T_2^{\mathrm{II}}(0)$ will be denoted as the slow body wave.

4.2. *The precursor*

The contribution from the simple pole p_0^{II} to the Green's function is analyzed next. The location of the leftmost point of intersection p_1^{II} of the modified Cagniard path with the real axis satisfies the relation (cf. eq. (51))

$$[B^2(q)-p^2]^2=16(|x_3|/r)c^{-3}p \quad \text{at } p=p_1^{\mathrm{II}}(q). \tag{73}$$

Upon substituting p_0^{II} (cf. eq. (65)) into eq. (73), the value q_0^{II} for q is found at which p_0^{II} and p_1^{II} coincide, viz.,

$$(q_0^{\mathrm{II}})^2=(4/3c^2)[(4/27)(r/|x_3|)^2-1]. \tag{74}$$

Note that q_0^{II} is real only if $r\geqslant\frac{3}{2}\sqrt{3}|x_3|$. Differentiating eq. (73) with respect to q yields

$$\partial_q p=\frac{q}{p+([4|x_3|/rc^3]/[B^2(q)-p^2])} \quad \text{for } p=p_1^{\mathrm{II}}(q). \tag{75}$$

Since $p_1^{\mathrm{II}}(q)<B(q)$, eq. (75) leads to

$$\partial_q p_1^{\mathrm{II}}(q)\leqslant\frac{q}{p_1^{\mathrm{II}}(q)} \tag{76}$$

when $q>0$. Further, from eq. (65) it is clear that

$$\partial_q p_0^{\mathrm{II}}(q)=\frac{q}{p_0^{\mathrm{II}}(q)}. \tag{77}$$

Hence, when $q=q_0^{\mathrm{II}}$, $\partial_q p_0^{\mathrm{II}}(q)>\partial_q p_1^{\mathrm{II}}(q)$, so that the pole p_0^{II} lies to the left of p_1^{II} if $q^2<(q_0^{\mathrm{II}})^2$. In view of eq. (74), this inequality cannot be satisfied when $r<\frac{3}{2}\sqrt{3}|x_3|$. Hence, the pole contributes only when $r>\frac{3}{2}\sqrt{3}|x_3|$. Evaluating the residue, the relevant contribution is found to be

$$\hat{G}_0^{\mathrm{II}}=\frac{2}{9\pi c}\int_{q=0}^{q_0^{\mathrm{II}}}\frac{\exp[-sr(q^2+4/3c^2)^{1/2}]}{(q^2+4/3c^2)^{1/2}}\,\mathrm{d}q, \tag{78}$$

which, upon replacing $r(q^2+4/3c^2)^{1/2}$ by τ, takes the form

$$\hat{G}_0^{\mathrm{II}}=\frac{2}{9\pi c}\int_{\tau=T_{0,1}^{\mathrm{II}}}^{T_{0,2}^{\mathrm{II}}}\frac{\exp(-s\tau)}{(\tau^2-4r^2/3c^2)^{1/2}}\,\mathrm{d}\tau, \tag{79}$$

in which

$$T_{0,1}^{\mathrm{II}}=(2/\sqrt{3})(r/c) \quad \text{and} \quad T_{0,2}^{\mathrm{II}}=(4r/9|x_3|)(r/c). \tag{80}$$

On account of Lerch's theorem on the uniqueness of the Laplace transform of a causal time function, taken at positive real values of s, the time-domain counterpart G_0^{II} of $\hat{G}_0^{\mathrm{II}}$ then follows as

$$G_0^{\mathrm{II}}=\frac{2}{9\pi c[t^2-(T_{0,1}^{\mathrm{II}})^2]^{1/2}}[H(t-T_{0,1}^{\mathrm{II}})-H(t-T_{0,2}^{\mathrm{II}})]. \tag{81}$$

This contribution (see Fig. 11), which is only present if $r>|x_3|\frac{3}{2}\sqrt{3}$, is to be added to the contribution from the modified Cagniard path eq. (69). It can be interpreted as a head-wave-like precursor to the fast and slow body waves.

4.3. *The case $r=0$*

For an observation position straight above or below the source, we need the expression for the Green's function at $r=0$. In view of the occurrence of the Dirac distribution in eq. (68), the limit as $r\downarrow 0$ has to be

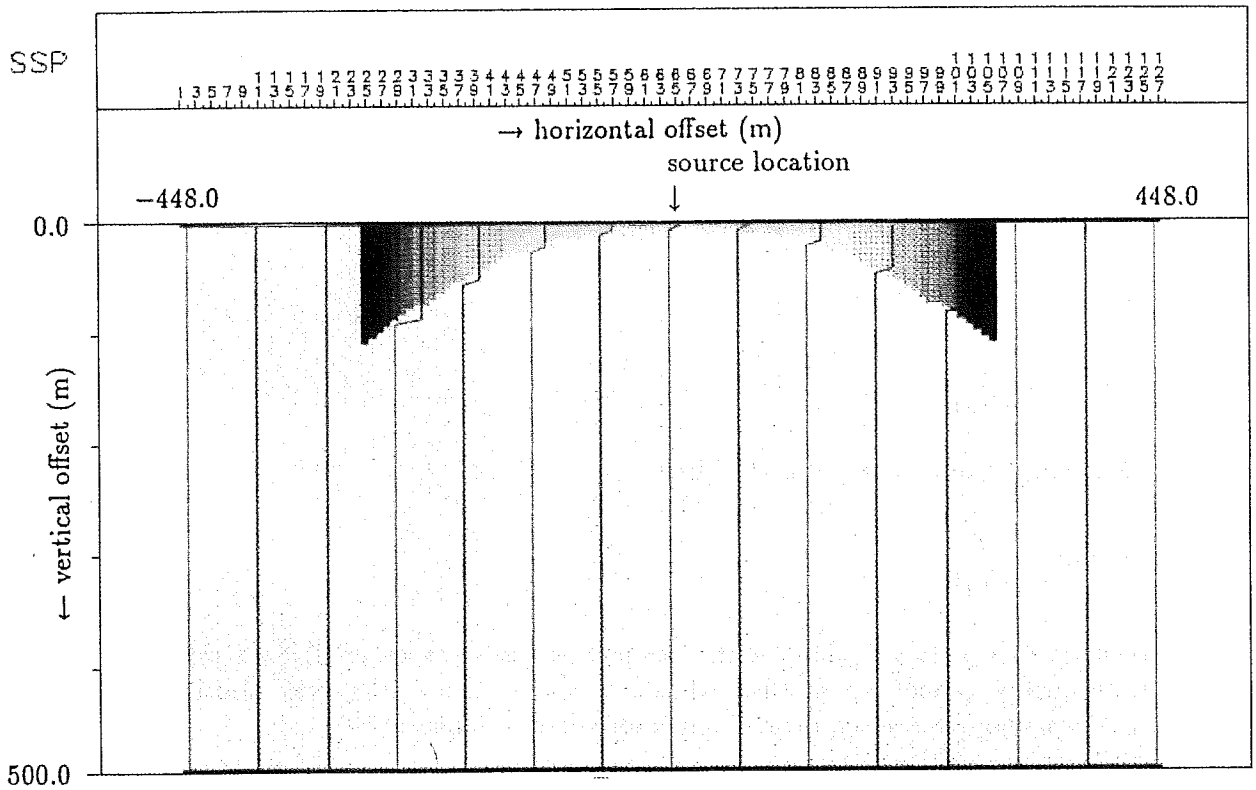

Fig. 11. Snapshot of the pole contribution to the Green's function in space for $x_3\geqslant 0$ in the second-order Thiele approximation; $c=$ 750 m/s, $t=0.450$ s. (The horizontal offsets are numbered sequentially.)

taken with care, since the substitution of the value $r=0$ in the Fourier representation for the Green's function leads to a divergent integral whose interpretation as a Dirac distribution is not obvious. To circumvent this difficulty, we leave the term in eq. (68) containing the Dirac distribution intact and take in the subsequent terms in the expression the limit $r\downarrow 0$. The corresponding contour then tends, in a non-uniform manner, to the imaginary p-axis (the points at infinity in the complex p-plane have to be identified with one another). When $r=0$, the cubic equation for the modified Cagniard path reduces to a quadratic one (cf. eq. (47)); the latter is solved by

$$p^{\mathrm{II}}(\tau, q)=\mathrm{i}B(q)\left[\frac{\tau-T_1^{\mathrm{II}}(q)}{T_2^{\mathrm{II}}-\tau}\right]^{1/2} \tag{82}$$

for $r=0$, $T_1^{\mathrm{II}}(q)<\tau<T_2^{\mathrm{II}}$, together with its complex conjugate, in which

$$T_1^{\mathrm{II}}(q)=\frac{3|x_3|}{c}\left[1-\frac{A^2}{B^2(q)}\right] \tag{83}$$

and

$$T_2^{\mathrm{II}}=\frac{3|x_3|}{c}. \tag{84}$$

For this case, the contour coincides with the imaginary axis and closes at infinity as opposed to the contours for $r\neq 0$ at which p^{II} remains bounded. The path of integration intersects the real axis at the origin where $\tau=T_1^{\mathrm{II}}(q)$ and tends to infinity as $\tau\uparrow T_2^{\mathrm{II}}$. The relation inverse to eq. (83) is $q=Q_1^{\mathrm{II}}(\tau)$, with

$$Q_1^{\mathrm{II}}(\tau)=\frac{2}{c}\left[\frac{\tau-|x_3|/c}{3|x_3|/c-\tau}\right]^{1/2} \tag{85}$$

for $|x_3|/c<\tau<3|x_3|/c$, while eq. (85) implies that only the first integral of eq. (69) contributes. This integral can be evaluated, and the Green's function reduces to

$$\lim_{r\downarrow 0}\left[G_{\mathrm{C}}^{\mathrm{II}}(r, x_3, t)-\frac{c}{6}(t-3|x_3|/c)H(t-3|x_3|/c)\frac{1}{r}\delta(r)\right]=\frac{1}{\pi ct}\frac{x_3^2}{(3|x_3|-ct)^2}[H(t-|x_3|/c)-H(t-3|x_3|/c)]. \tag{86}$$

4.4. The case $x_3=0$

In the case $x_3=0$, the modified Cagniard contour coincides with the positive real p-axis. In view of the analyticity of the integrand away from the pole, when $x_3=0$, we have a contribution from the arc at infinity and a contribution from the pole. The latter is given by (cf. eq. (78))

$$\hat{G}_0^{\mathrm{II}}=\frac{2}{9\pi c}\int_{q=0}^{\infty}\frac{\exp[-sr(q^2+4/3c^2)^{1/2}]}{(q^2+4/3c^2)^{1/2}}\,\mathrm{d}q. \tag{87}$$

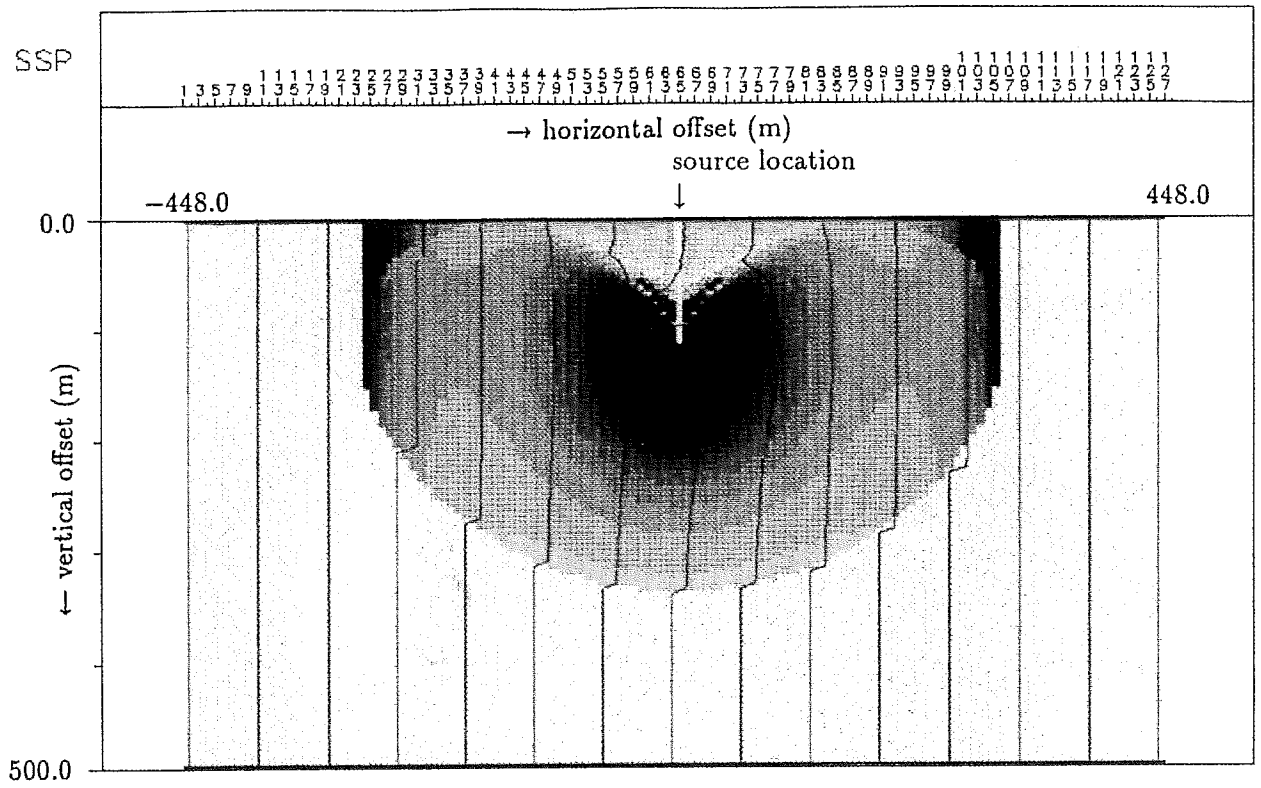

Fig. 12. Snapshot of the total Green's function in space for $x_3 \geqslant 0$ in the second-order Thiele approximation; $c = 750$ m/s, $t = 0.450$ s. (The singular part at $r = 0$ is not shown. The horizontal offsets are numbered sequentially.)

The space-time counterpart is found to be (cf. eq. (81))

$$G_0^{\mathrm{II}} = \frac{2}{9\pi c[t^2 - (T_{0,1}^{\mathrm{II}})^2]^{1/2}} H(t - T_{0,1}^{\mathrm{II}}), \tag{88}$$

in which $T_{0,1}^{\mathrm{II}}$ is given in eq. (80). The total Green's function is then (cf. eq. (69))

$$G^{\mathrm{II}} = G_0^{\mathrm{II}} + \frac{c}{6} tH(t)\delta(x_1, x_2). \tag{89}$$

Figure 12 shows a snapshot in space of the total Green's function $G_C^{\mathrm{II}} + G_0^{\mathrm{II}}$ for $x_3 \geqslant 0$.

4.5. *Partial differential equation for* G^{II}

By differentiating the right-hand side of eq. (46) twice with respect to x_3, and using that under the transformations of eqs. (5) and (6) we have $\partial_t \to s$ and $\partial_\mu \to -is\alpha_\mu$, we can reconstruct the partial differential equation that G^{II} satisfies, viz.,

$$\{c^{-2}\partial_t^2(\partial_3 + c^{-1}\partial_t) - [(1/4)\partial_3 + (3/4c)\partial_t]\partial_\mu\partial_\mu\}\{c^{-2}\partial_t^2(\partial_3 - c^{-1}\partial_t) - [(1/4)\partial_3 - 3/4c)\partial_t]\partial_\nu\partial_\nu\}G^{\mathrm{II}}$$
$$= -[c^{-2}\partial_t^2 - (1/4)\partial_\lambda\partial_\lambda]^2\delta(x_1, x_2, x_3)H(t). \tag{90}$$

The first partial differential operator in braces on the left-hand side of eq. (90) is the second-order approximation to the wave operator for a wave propagating in the direction of increasing x_3; the second partial differential operator in braces on the left-hand side of eq. (90) is the second-order approximation to the wave operator for a wave propagating in the direction of decreasing x_3 [11].

5. Arrival times as functions of horizontal offset

A Thiele approximation of the vertical slowness is accurate for small values of α_1 and α_2 (cf. eq. (7)). In this sense, it aims to approximate wave propagation in the vertical direction. How the results of this approximation compare with the ones of the asymptotic ray solution along a vertical ray is the topic of this and the next sections. In the present section, relations between horizontal offset and arrival time are derived for the different approximations. We keep $|x_3|$ fixed and let r vary. The vertical travel, or intercept, time is denoted by $T_{\min}=|x_3|/c$, and the arrival time by T.

For the *exact* wave motion only a single body wave is present and its arrival time satisfies the equation (cf. eq. (4))

$$T^2-(r/c)^2=T_{\min}^2, \tag{91}$$

which leads to

$$r(T)=c(T^2-T_{\min}^2)^{1/2} \quad \text{for } T\geqslant T_{\min}. \tag{92}$$

This is also the relation predicted by ray theory (where straight rays emanate from the source to the point of observation).

For the *first-order* Thiele approximation there is a single bodywave whose arrival time satisfies the equation (cf. eq. (33))

$$(T_{\min}-T/2)^2+r^2/2c^2=(T/2)^2, \tag{93}$$

the solution of which is

$$r^{\mathrm{I}}(T)=c[2T_{\min}(T-T_{\min})]^{1/2} \quad \text{for } T\geqslant T_{\min}. \tag{94}$$

In addition, there is a head-wave-like precursor whose arrival time is given by (cf. eq. (38)

$$r_{0,1}^{\mathrm{I}}(T)=cT/\sqrt{2} \quad \text{for } T\geqslant 2T_{\min}; \tag{95}$$

this precursor is only present if $r>R_0^{\mathrm{I}}$, where $R_0^{\mathrm{I}}=cT_{\min}\sqrt{2}$ (see Fig. 13).

For the *second-order* Thiele approximation we have eq. (64),

$$T^4-10T_{\min}T^3+4\left[9T_{\min}^2-2\left(\frac{r}{c}\right)^2\right]T^2-6T_{\min}\left[9T_{\min}^2+4\left(\frac{r}{c}\right)^2\right]T+27T_{\min}^4+36T_{\min}^2\left(\frac{r}{c}\right)^2+16\left(\frac{r}{c}\right)^4=0, \tag{96}$$

the two real-valued positive solutions of which are

$$r_1^{\mathrm{II}}(T)=\left[-\frac{1}{32}(\mathscr{F}-\Delta_r^{1/2})\right]^{1/2} \quad \text{for } T\geqslant T_{\min} \tag{97}$$

for the fast body wave, and

$$r_2^{\mathrm{II}}(T)=\left[-\frac{1}{32}(\mathscr{F}+\Delta_r^{1/2})\right]^{1/2} \quad \text{for } T>3T_{\min} \tag{98}$$

for the slow body wave, where

$$\mathscr{F}=-4c^2[2T^2+6T_{\min}T-9T_{\min}^2] \tag{99}$$

and

$$\Delta_r=-16c^4T_{\min}^4[3-4(T/T_{\min})]^3. \tag{100}$$

At $T=3T_{\min}$ there is a spatial δ-function singularity on the vertical axis, i.e., right at the cusps of the wave front of the slow wave. In addition, there is a head-wave-like precursor whose arrival time is given by (cf. eq. (80))

$$r_{0,1}^{\mathrm{II}}(T)=(\sqrt{3}/2)cT \quad \text{for } T\geqslant 3T_{\min}, \tag{101}$$

which is present only if $r>R_0^{\mathrm{II}}$ with $R_0^{\mathrm{II}}=cT_{\min}\frac{3}{2}\sqrt{3}$ (see Fig. 14).

It is noted that the vertical travel times associated with the (fast) body wave in the first- and second-order Thiele approximations are exact. Furthermore, it follows that $R_0^{\mathrm{II}}>R_0^{\mathrm{I}}$.

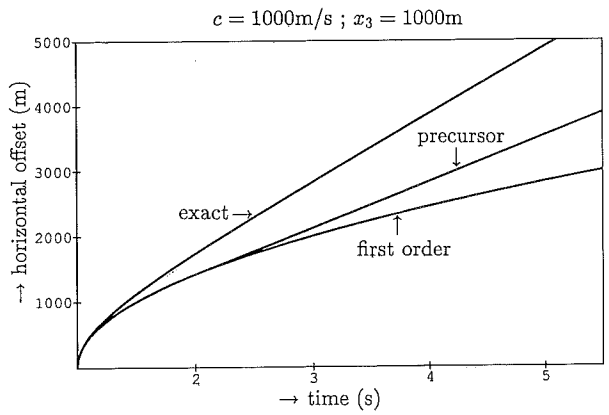

Fig. 13. Travel time vs. horizontal offset (diffraction) curves associated with the arrivals of the exact and first-order Thiele-approximated Green's functions.

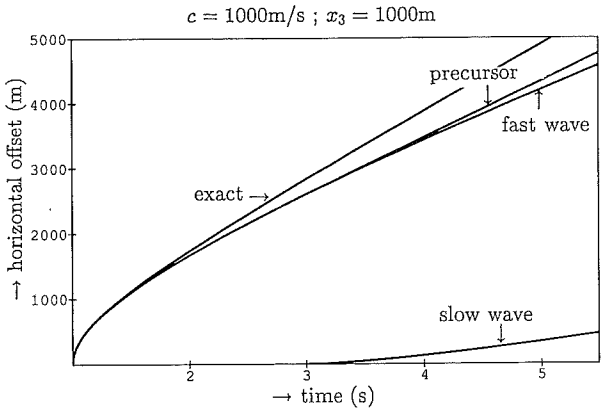

Fig. 14. Travel time vs. horizontal offset (diffraction) curves associated with the arrivals of the exact and second-order Thiele-approximated Green's functions.

6. The local behavior of the waves near the wave fronts in the vertical direction

In this section we compare the local behaviors of the waves near the wave fronts in the vertical direction for the exact Green's function and its first- and second-order Thiele approximations.

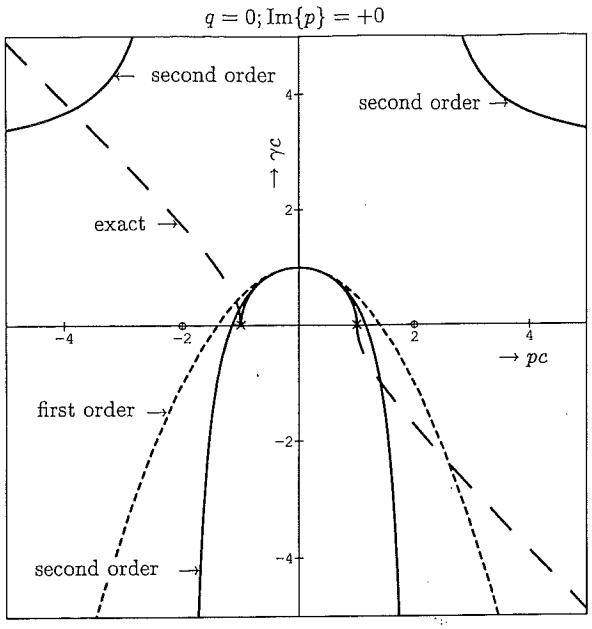

Fig. 15. The exact and the first- and second-order Thiele-approximated vertical slownesses along the real horizontal slowness axis. The circles indicate the pole locations of the second-order Thiele approximant; the crosses indicate the branch points of the exact vertical slowness; the dashes in the exact case indicate purely imaginary values of the vertical slowness. (When r is large compared to $|x_3|$, the exact modified Cagniard path stays close to the real horizontal slowness (p-) axis.)

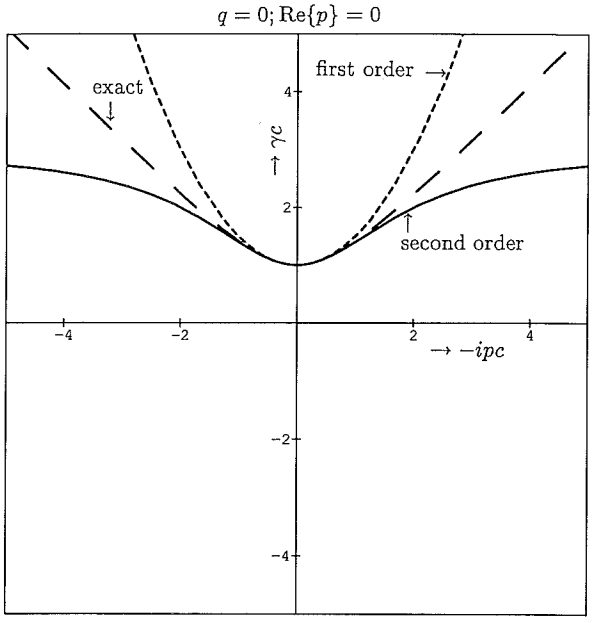

Fig. 16. The exact and the first- and second-order Thiele-approximated vertical slownesses along the imaginary horizontal slowness axis. (When r is small compared to $|x_3|$, the exact modified Cagniard path stays close to the imaginary horizontal slowness (p-) axis.)

The *exact* Green's function at $\{0, 0, x_3\}$ reduces to (cf. eq. (4))

$$G(0, 0, x_3, t) = \frac{1}{4\pi|x_3|} H(t - |x_3|/c). \tag{102}$$

The *first-order* Thiele approximation at $\{0, 0, x_3\}$ yields (cf. eq. (35))

$$G^{\mathrm{I}}(0, 0, x_3, t) = \frac{1}{4\pi ct} H(t - |x_3|/c). \tag{103}$$

Replacing t in the denominator of eq. (103) by $t = |x_3|/c + (t - |x_3|/c)$, and using a Taylor expansion of the resulting expression about the arrival time $t = |x_3|/c$, yields

$$G^{\mathrm{I}}(0, 0, x_3, t) = \left[\frac{1}{4\pi|x_3|} - \frac{c}{4\pi x_3^2}(t - |x_3|/c) + \mathrm{O}[(t - |x_3|/c)^2]\right] H(t - |x_3|/c). \tag{104}$$

The right-hand side is the ray series expansion along a vertical ray. (The ray series expansion of the first-order Thiele approximation in an arbitrary direction is discussed by Holden and Gorman [36].) The leading term in eq. (104) coincides with the exact result (cf. eq. (102)), whereas the next-order term already deviates from it. This result could also have been predicted from the parabolic equation in ray-centered coordinates occurring in the paraxial ray theory (see, e.g., [37]).

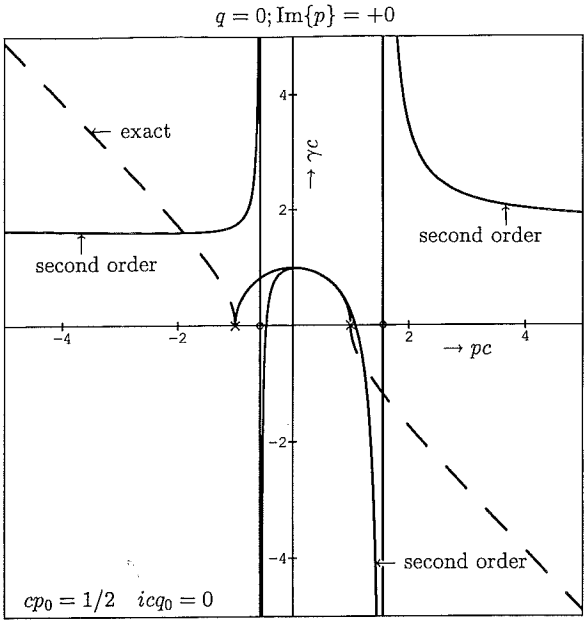

Fig. 17. The exact and second-order Thiele-approximated vertical slownesses along the real horizontal slowness axis for an oblique direction of propagation. The circles indicate the pole locations of the second-order Thiele approximant; the crosses indicate the branch points of the exact vertical slowness; the dashes in the exact case indicate purely imaginary values of the vertical slowness.

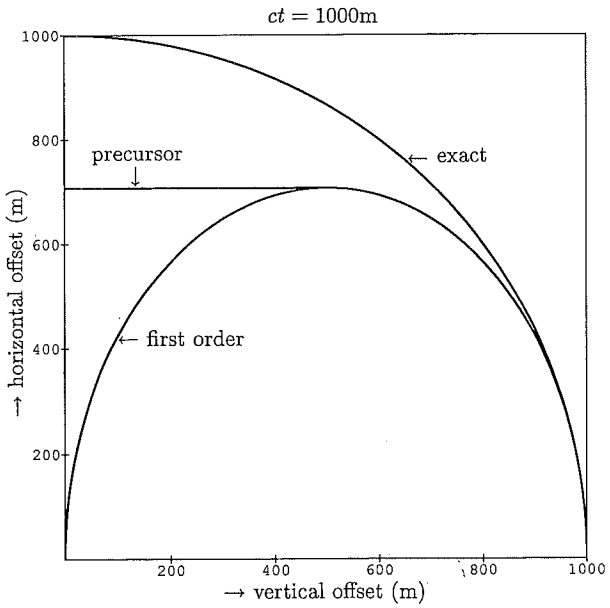

Fig. 18. The wave fronts associated with the arrivals of the exact and first-order Thiele-approximated Green's functions.

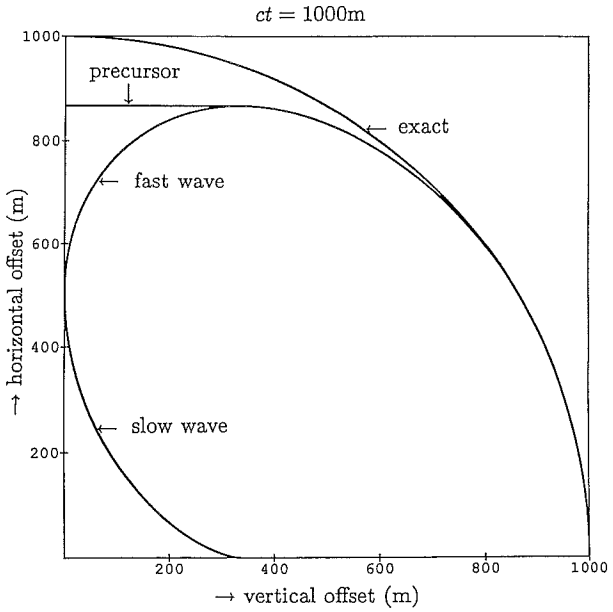

Fig. 19. The wave fronts associated with the arrivals of the exact and second-order Thiele-approximated Green's functions.

In the *second-order* Thiele approximation at $\{0, 0, x_3\}$ the Green's function reduces to (cf. eq. (86))

$$\lim_{(x_1, x_2) \to (0, 0)} \left[G_C^{II}(x_1, x_2, x_3, t) - \frac{c}{6} (t - 3|x_3|/c) H(t - 3|x_3|/c) \delta(x_1, x_2) \right]$$

$$= \frac{1}{\pi c t} \frac{x_3^2}{(3|x_3| - ct)^2} [H(t - |x_3|/c) - H(t - 3|x_3|/c)]. \tag{105}$$

Replacing t in the denominator of eq. (105) by $t = |x_3|/c + (t - |x_3|/c)$, and using a Taylor expansion of the resulting expression about the arrival time $t = |x_3|/c$ of the fast body wave, yields

$$G^{II}(0, 0, x_3, t) = \left[\frac{1}{4\pi |x_3|} + \frac{3c^2}{16\pi |x_3|^3} (t - |x_3|/c)^2 + O[(t - |x_3|/c)^3] \right] H(t - |x_3|/c), \tag{106}$$

which shows that now the first two orders are exact (cf. eq. (102)).

The arrival-time curves and the snapshots (see Figs. 1, 6 and 12) show that the accuracy of asymptotic ray theory is achieved along the vertical ray only; in oblique directions of propagation there is a discrepancy. In oblique directions a better approximation is found if the vertical slowness is expanded about the actual direction of the ray trajectory connecting the source and receiver. Such an approach requires an adapted form of Thiele's expansion about an oblique direction of propagation, which is discussed in Appendix A.

7. Concluding remarks

The foregoing analysis has revealed the general consequences that spectral-domain Thiele approximations for the vertical wave slowness have for the corresponding space-time domain wave motion. The most striking feature is that Thiele approximations lead to a number of non-physical artefacts that do not occur in the exact wave motion. First of all, for even-order approximants, a singularity in the wave motion is observed right above and below the source, which is absent in both the exact wave motion and in odd-order approximants. Further, for horizontal offsets that are large compared to the vertical offset, non-physical head-wave-like precursors occur. In addition, any Thiele approximant of order higher than one introduces "slow" waves, which again are absent in the exact wave motion (see also Collins [38]). In the odd-order approximations, however, they never occur along a direction of propagation which lies interior to a certain cone centered on the vertical axis.

On the other hand, Thiele approximations reproduce amplitudes along the "vertical ray" as accurately as the asymptotic ray theory does. However, in contrast to asymptotic ray theory, the Thiele-approximated wave theory automatically initializes the ray amplitudes in the immediate neighborhood of the source.

In conclusion, one can state that Thiele approximations are sufficiently accurate inside a cone for not too large horizontal-versus-vertical offset ratios and in a restricted time window, i.e., in the neighborhood of the arrival of the physical body wave. Further, in view of the associated non-physical singularities straight above and below the source, the even-order approximants are to be avoided.

Acknowledgement

The authors would like to thank Professor P.M. van den Berg, Faculty of Electrical Engineering, and Dr. J.T. Fokkema, Faculty of Mining and Petroleum Engineering, Delft University of Technology, for their helpful discussions.

References

[1] M.A. Leontovich and V.A. Fock, "Solution of the problem of propagation of electromagnetic waves along the earth's surface by the method of parabolic equation", *J. Phys. U.S.S.R. 10*, 13–24 (1946).
[2] V.A. Fock, "The field of a plane wave near the surface of a conducting body", *J. Phys. U.S.S.R. 10*, 399–409 (1946).
[3] H. Bremmer, "On the asymptotic evaluation of diffraction integrals with special view to the theory of defocusing and optical contrast", *Physica 18*, 469–485 (1952).
[4] V.I. Klyatskin and V.I. Tatarskii, 'The parabolic equation approximation for propagation of waves in a medium with random inhomogeneities", *Sov. Phys. JETP 31*, 335–339 (1970).
[5] J.F. Claerbout, "Coarse grid calculations of waves in inhomogeneous media with application to delineation of complicated seismic structure", *Geophys. 35*, 407–418 (1970).
[6] S.T. McDaniel, "Parabolic approximations for underwater sound propagation", *J. Acoust. Soc. Am. 58*, 1178–1185 (1975).
[7] F.D. Tappert, "The parabolic approximation method", in: J.B. Keller and J.S. Papadakis (Eds.), Wave Propagation in Underwater Acoustics, *Lecture Notes in Physics No. 70*, Springer, New York (1977) pp. 224–287.
[8] D. Ristow, 3D downward extrapolation of seismic data in particular by finite difference methods, PhD thesis, University of Utrecht, Utrecht, 1980.
[9] Z. Ma, "Finite-difference migration with higher order approximation", *Oil Geophys. Prosp. China 1*, 6–15 (1982).
[10] M.W. Lee and S.Y. Suh, "Optimization of one-way wave equations", *Geophys. 50*, 1634–1637 (1985).
[11] P.G. Kelamis and E. Kjartansson, "Forward modeling in the frequency-space domain", *Geophys. Prosp. 33*, 252–262 (1985).
[12] R.W. Graves and R.W. Clayton, "Modeling acoustic waves with paraxial extrapolators", *Geophys. 55*, 306–319 (1990).
[13] J.P. Corones and R.J. Krueger, 'Higher-order parabolic approximations to time-independent wave equations", *J. Math. Phys. 24*, 2301–2304 (1983).
[14] A.J. Berkhout, 'Steep dip finite difference migration", *Geophys. Prosp. 27*, 196–213 (1979).
[15] R.R. Greene, "The rational approximation to the acoustic wave equation with bottom interaction", *J. Acoust. Soc. Am. 76*, 1764–1773 (1984).
[16] P. Joly, Etude mathématique de l'approximation parabolique de l'équation des ondes en milieu stratifié, Rapport No. 299 de l'Institut National de Recherche en Informatique et en Automatique, 1984.
[17] A. Bamberger, B. Engquist, L. Halpern and P. Joly, Construction et analyse d'approximations paraxiales en milieu hétérogène, Rapport No. 114 du Centre de Mathématiques Appliquées de l'Ecole Polytechnique, 1984.
[18] A. Bamberger, B. Engquist, L. Halpern and P. Joly, "Higher order paraxial wave equation approximations in heterogeneous media", *SIAM J. Appl. Math. 48*, 129–154 (1988).
[19] R. Burridge, "The singularity on the plane lids of the wave surface of elastic media with cubic symmetry", *Quart. J. Mech. Appl. Math. XX*, 41–56 (1967).
[20] D.R. Palmer, "Eikonal approximation and the parabolic equation", *J. Acoust. Soc. Am. 60*, 343–354 (1976).
[21] L. Fishman and J.J. McCoy, "Derivation and application of extended parabolic wave theories I. The factorized Helmholtz equation", *J. Math. Phys. 25*, 285–296 (1984).
[22] J. Gazdag, "Wave equation migration with the phase shift method", *Geophys. 43*, 1342–1351 (1978).
[23] J. Gazdag and P. Sguazzero, "Migration of seismic data by phase shift plus interpolation", *Geophys. 49*, 124–131 (1984).
[24] L. Halpern and L.N. Trefethen, "Wide-angle one-way wave equations", *J. Acoustic. Soc. Am. 86*, 1397–1404 (1988).
[25] Zhang Guan-quan, Zhang Shu-lun, Wang Ying-xiang and Liu Chau-ying, "A new algorithm for finite-difference migration of steep dips", *Geophys. 53*, 167–175 (1988).
[26] E.A. Polyanskii, "Relationship between the solutions of the Helmholtz and Schrödinger equations", *Sov. Phys. Acoust. 20*, 90 (1974).
[27] J.A. De Santo, "Relation between the solutions of the Helmholtz and the parabolic equations for sound propagation", *J. Acoust. Soc. Am. 62*, 295–297 (1977).
[28] A.T. de Hoop, "A modification of Cagniard's method for solving seismic pulse problems", *Appl. Sci, Res. B8*, 349–356 (1960).
[29] A.T. de Hoop, "Large-offset approximations in the modified Cagniard method for computing synthetic seismograms: a survey", *Geophys. Prosp. 36*, 465–477 (1988).

[30] J.D. Achenbach, *Wave Propagation in Elastic Solids*, North-Holland, Amsterdam (1973).
[31] J. Miklowitz, *The Theory of Elastic Waves and Wave Guides*, North-Holland, Amsterdam (1978).
[32] K. Aki and P.G. Richards, *Quantitative Seismology*, Freeman, San Francisco (1980).
[33] J.H.M.T. van der Hijden, *Propagation of Transient Elastic Waves in Stratified Anisotropic Media*, North-Holland, Amsterdam (1987).
[34] I.G. Petrowsky, "On the diffusion of waves and the lacunas for hyperbolic equations", *Mat. Sb. 17*, 289–370 (1945).
[35] D.V. Widder, *The Laplace Transform*, Princeton University Press, Princeton (1946).
[36] K.L. Holden and A.D. Gorman, "Caustics and the parabolic equation", *Wave Motion 11*, 33–39 (1989).
[37] V. Červený and I. Pšenčik, "Gaussian beams and paraxial ray approximation in three-dimensional elastic inhomogeneous media", *J. Geophys. 53*, 1–15 (1983).
[38] M.D. Collins, "Applications and time-domain solution of higher-order parabolic equations in underwater acoustics", *J. Acoust. Soc. Am. 86*, 1097–1102 (1989).
[39] T.N. Thiele, *Interpolationsrechnung*, Teubner, Leipzig (1909) §41.
[40] F.B. Hildebrand, *Introduction to Numerical Analysis*, McGraw-Hill, New York (1956).
[41] W.B. Jones and W.J. Thron, *Continued Fractions. Analytic Theory and Applications*, Addison-Wesley, Reading (1980).
[42] H. Padé, "Sur la représentation approchée d'une fonction par des fractions rationelles", *Ann. Sci. Ecole Norm. Sup. 9*, 1–93 (1892).
[43] L.A. Lyusternik and A.R. Yanpol'skii, *Mathematical Analysis. Functions, Limits, Series, Continued Fractions*, Pergamon, Oxford (1965).
[44] A.N. Khovanskii, *The Application of Continued Fractions and their Generalizations to Problems in Approximation Theory*, Noordhoff, Groningen (1963).
[45] I.S. Sokolnikoff and E.S. Sokolnikoff, *Higher Mathematics for Engineers and Physicists*, McGraw-Hill, New York (1941).
[46] D.E. Dobbs and R. Hanks, *A Modern Course on the Theory of Equations*, Polygonal Publishing House, Passaic (1980).
[47] R. Courant and D. Hilbert, *Methods of Mathematical Physics*, Volume 2, Wiley, New York (1989).

Appendix A. Thiele's continued-fraction approximations

In this appendix we investigate general Thiele continued-fraction approximations of the vertical slowness. First, Thiele's formula is summarized; next, it is applied to the vertical slowness. Special attention is paid to the higher-order Thiele approximations, which are written as a sum of terms resembling first- and second-order like approximants. Owing to this property, the waves associated with the higher-order approximations in an unbounded homogeneous medium can be expressed in terms of waves in a quasi-multilayer configuration, the vertical slownesses in each individual layer being replaced by first- and second-order-like approximants. Second, Thiele's formula is extended to two dimensions, which allows for an expansion about an oblique direction of propagation.

The Thiele's continued-fraction approximation [39, 40] of a function $g(x)$ about $x=x_0$ is given by

$$g(x)=a_0+\cfrac{x-x_0}{a_1+\cfrac{x-x_0}{a_2+\cfrac{x-x_0}{a_3+\cdots}}} \tag{A.1}$$

with coefficients

$$a_0=g(x_0), \qquad a_k=k/\frac{\mathrm{d}\rho_{k-1}}{\mathrm{d}x}(x_0) \quad \text{for } k=1,2,\ldots, \tag{A.2}$$

where the function $\rho_k(x)$ follows from the recursion relation

$$\rho_{-1}(x)=0, \qquad \rho_0(x)=g(x), \quad \rho_k(x)=\rho_{k-2}(x)+k/\frac{\mathrm{d}\rho_{k-1}}{\mathrm{d}x}(x) \quad \text{for } k=1,2,\ldots \tag{A.3}$$

Notice that $a_k=\rho_k(x_0)-\rho_{k-2}(x_0)$. The function ρ_k is called the kth reciprocal derivative of g. It is assumed that all reciprocal derivatives exist. We denote by

$$g_k(x)=\cfrac{x-x_0}{a_1+\cfrac{x-x_0}{\ddots+\cfrac{x-x_0}{a_{k-1}+\cfrac{x-x_0}{a_k}}}} \tag{A.4}$$

for $k=1,2,\ldots$ the kth convergent of the continued fraction. Equation (A.1) is the confluent expansion that follows from the reciprocal-difference interpolation scheme applied to $g=g(x)$ through the limit of $k+1$ coinciding abscissas. Then, the difference between g and the kth convergent of the fraction $g(x_0)+g_k$ vanishes at x_0 for its first k derivatives. As such, eq. (A.1) can be seen as an alternative to the Taylor expansion of $g=g(x)$ about $x=x_0$.

Expansion about the vertical direction of propagation

Applying the expansion to $g(x^2)=(1-x^2)^{1/2}$, as it occurs in the spectral-domain vertical slowness, considered as a function of x^2, about $x^2=x_0^2=0$ (and hence away from the branch points at $x^2=1$), we get

$$(1+g_k)\to g \quad \text{as } k\to\infty, \tag{A.5}$$

with

$$g_0=0, \qquad g_{k+1}=\frac{-x^2}{2+g_k} \tag{A.6}$$

for $k=0,1,2,\ldots$. The resulting continued fraction is classified as an S-fraction [41]. Now, the general formula for an even-order approximation can be written as

$$\frac{1}{2}g_{2m}=\frac{\sum_{i=1}^{m} a_i^{(m)}(-x^2/4)^i}{\sum_{j=0}^{m} b_j^{(m)}(-x^2/4)^j}, \quad \text{for } m\geqslant 1, \tag{A.7}$$

whereas the general formula for an odd-order approximation can be written as

$$\frac{1}{2}g_{2m-1}=\frac{\sum_{i=1}^{m} c_i^{(m)}(-x^2/4)^i}{\sum_{j=0}^{m-1} d_j^{(m)}(-x^2/4)^j}, \quad \text{for } m\geqslant 1. \tag{A.8}$$

Equations (A.7) and (A.8) are known as the (m,m) and $(m,m-1)$ entries in the Padé table of g relative to 0 [42]. (The Padé table also contains more general rational approximations.) The first $2m$ (for even

order) or $2m-1$ (for odd order) derivatives coincide with the corresponding derivatives of g at 0. Relying on the relation

$$\binom{k+1}{j}=\binom{k}{j}+\binom{k}{j-1},$$

it can be shown by induction that (cf. eq. (A.6))

$$a_i^{(m)}=\binom{2m-i}{i-1}, \tag{A.9}$$

$$b_j^{(m)}=\binom{2m-j}{j}, \tag{A.10}$$

$$c_i^{(m)}=\binom{2m-1-i}{i-1}, \tag{A.11}$$

$$d_j^{(m)}=\binom{2m-1-j}{j}. \tag{A.12}$$

From eqs. (A.9)–(A.12), it follows that

$$a_1^{(1)}=1, \quad b_0^{(1)}=1, \quad b_1^{(1)}=1,$$

$$a_1^{(2)}=1, \quad a_2^{(2)}=2, \quad b_0^{(2)}=1, \quad b_1^{(2)}=3, \quad b_2^{(2)}=1,$$

$$\ldots$$

and

$$c_1^{(1)}=1, \quad d_0^{(1)}=1,$$

$$c_1^{(2)}=1, \quad c_2^{(2)}=1, \quad d_0^{(2)}=1, \quad d_1^{(2)}=2,$$

$$\ldots$$

which are all positive. It is observed that the sequence $\{u_n\}$ with $u_{2m-1}=\sum_{i=1}^{m} c_i^{(m)}$ and $u_{2m}=\sum_{i=1}^{m} a_i^{(m)}$ ($m=1, 2, \ldots$) consists of the Fibonacci numbers [43]. A similar observation holds for the sequence consisting of the remaining coefficients: $u_{2m}=\sum_{i=0}^{m-1} d_i^{(m)}$ and $u_{2m+1}=\sum_{i=0}^{m} b_i^{(m)}$.

The even orders for $m\geqslant 2$ can be decomposed into partial fractions as follows:

$$g_{2m}=(-x^2/2)\sum_{i=1}^{m}\frac{\alpha_i^{(m)}}{1+\beta_i^{(m)}(-x^2/4)}, \tag{A.13}$$

so that

$$1+g_{2m}=\frac{1}{m}\sum_{i=1}^{m}\frac{1+(\beta_i^{(m)}+2m\alpha_i^{(m)})(-x^2/4)}{1+\beta_i^{(m)}(-x^2/4)}, \tag{A.14}$$

where

$$\alpha_j^{(m)}=\frac{\prod_{p=1}^{m-1}\left[\cos^2\left(\frac{j\pi}{2m+1}\right)-\cos^2\left(\frac{p\pi}{2m}\right)\right]}{\prod_{q=1,q\neq j}^{m}\left[\cos^2\left(\frac{j\pi}{2m+1}\right)-\cos^2\left(\frac{q\pi}{2m+1}\right)\right]} \tag{A.15}$$

for $j=1,\ldots,m$ and

$$\beta_j^{(m)}=4\cos^2\left(\frac{j\pi}{2m+1}\right) \tag{A.16}$$

for $j=1,\ldots,m$. Hence

$$\alpha_1^{(2)}=\frac{5-\sqrt{5}}{10},\qquad \alpha_2^{(2)}=\frac{5+\sqrt{5}}{10},\qquad \beta_1^{(2)}=\frac{3+\sqrt{5}}{2},\qquad \beta_2^{(2)}=\frac{3-\sqrt{5}}{2},$$

...

Each term in eq. (A.14) is of the form of a second-order Thiele approximation (cf. eq. (44)).

The odd orders can be similarly decomposed into partial fractions as follows:

$$g_{2m+1}=(-x^2/2)\left\{\gamma_{m+1}^{(m)}+\sum_{i=1}^{m}\frac{\gamma_i^{(m)}}{1+\delta_i^{(m)}(-x^2/4)}\right\} \tag{A.17}$$

for $m\geqslant 1$, so that

$$1+g_{2m+1}=\frac{1}{m+1}\left\{1+2(m+1)\gamma_{m+1}^{(m)}(-x^2/4)+\sum_{i=1}^{m}\frac{1+(\delta_i^{(m)}+2(m+1)\gamma_i^{(m)})(-x^2/4)}{1+\delta_i^{(m)}(-x^2/4)}\right\}, \tag{A.18}$$

where

$$\gamma_j^{(m)}=\frac{\prod_{p=1}^{m}\left[\cos^2\left(\frac{j\pi}{2m+2}\right)-\cos^2\left(\frac{p\pi}{2m+1}\right)\right]}{\prod_{q=1,q\neq j}^{m+1}\left[\cos^2\left(\frac{j\pi}{2m+2}\right)-\cos^2\left(\frac{q\pi}{2m+2}\right)\right]}, \tag{A.19}$$

for $j=1,\ldots,m+1$ and

$$\delta_j^{(m)}=4\cos^2\left(\frac{j\pi}{2m+2}\right) \tag{A.20}$$

for $j=1,\ldots,m$. Hence

$$\gamma_1^{(1)}=\frac{1}{2},\qquad \gamma_2^{(1)}=\frac{1}{2},\qquad \delta_1^{(1)}=2,$$

...

The terms on the right-hand side of eq. (A.18) are of the form of the first- and second-order approximations (cf. eqs. (15) and (44)). In Figs. 15 and 16 the vertical slowness ($g=c\gamma$) as a function of horizontal slowness

($x=cp$) along the real (with $\mathrm{Im}\{x\}=+0$) and imaginary ($\mathrm{Re}\{x\}=0$) axes are shown for $x_0^2=0$, together with the corresponding first- and second-order Thiele approximations.

The asymptotic behaviors of the even- and odd-order approximations are essentially different, viz.,

$$g_{2m}=\mathrm{O}(1) \qquad \text{as } |x|\to\infty \tag{A.21}$$

whereas

$$g_{2m-1}=\mathrm{O}(x^2) \quad \text{as } |x|\to\infty. \tag{A.22}$$

Notice that the radius of convergence of the expansion is limited by the branch points of g at $x^2=1$ [44, pages 59–61]. From the convergence proof in the reference cited, the coefficients in eqs. (A.15), (A.16), (A.19) and (A.20) can be obtained.

Expansion about an oblique direction of propagation

To expand the vertical slowness about an oblique direction of propagation, a two-dimensional Thiele continued fraction approximation is employed. To arrive at the expansion about $\{x_0, y_0\}$, we substitute in the function $g(x, y)=(1-x^2-y^2)^{1/2}$

$$x-x_0=\alpha t \quad \text{and} \quad y-y_0=\beta t, \tag{A.23}$$

through which the two-dimensional expansion about $\{x_0, y_0\}$ is reduced to a one-dimensional one about $t=0$. The truncated continued fraction that results from the application of Thiele's formula is written as a rational function. The numerator and the denominator of the latter function are multiplied with t enough times so that α and β can be eliminated with the aid of eq. (A.23).

As long as $(x_0, y_0)\neq(0, 0)$, we get, e.g., for the fourth-order Thiele approximation:

$$\rho_0(t)=[1-(x_0+\alpha t)^2-(y_0+\beta t)^2]^{1/2}, \tag{A.24}$$

$$\rho_1(t)=-\frac{[1-(x_0+\alpha t)^2-(y_0+\beta t)^2]^{1/2}}{\alpha x_0+\beta y_0+(\alpha^2+\beta^2)t}, \tag{A.25}$$

$$\rho_2(t)=\rho_0(t)\,\frac{\alpha^2+\beta^2+2[\alpha x_0+\beta y_0+(\alpha^2+\beta^2)t]^2-(\beta x_0-\alpha y_0)^2}{\alpha^2+\beta^2-(\beta x_0-\alpha y_0)^2}, \tag{A.26}$$

$$\rho_3(t)=-\rho_1(t)\,\frac{2[\alpha x_0+\beta y_0+(\alpha^2+\beta^2)t]^2}{\alpha^2+\beta^2-2[\alpha x_0+\beta y_0+(\alpha^2+\beta^2)t]^2-(\beta x_0-\alpha y_0)^2}. \tag{A.27}$$

Hence,

$$a_1=-(1-x_0^2-y_0^2)^{1/2}\,\frac{1}{\alpha x_0+\beta y_0}, \tag{A.28}$$

$$a_2=(1-x_0^2-y_0^2)^{1/2}\,\frac{2(\alpha x_0+\beta y_0)^2}{\alpha^2+\beta^2-(\beta x_0-\alpha y_0)^2}, \tag{A.29}$$

$$a_3=(1-x_0^2-y_0^2)^{1/2}\,\frac{\alpha^2+\beta^2-(\beta x_0-\alpha y_0)^2}{(\alpha x_0+\beta y_0)[\alpha^2+\beta^2-(\beta x_0-\alpha y_0)^2-2(\alpha x_0+\beta y_0)^2]}, \tag{A.30}$$

$$a_4=(1-x_0^2-y_0^2)^{1/2}\frac{2[\alpha^2+\beta^2-(\beta x_0-\alpha y_0)^2-2(\alpha x_0+\beta y_0)^2]^2}{[\alpha^2+\beta^2-(\beta x_0-\alpha y_0)^2]^2}. \tag{A.31}$$

Writing the continued fraction as a rational function leads to

$$(1-x^2-y^2)^{1/2}=(1-x_0^2-y_0^2)^{1/2}+\frac{[a_2a_3a_4+(a_4+a_2)t]t}{a_1a_2a_3a_4+(a_1a_2+a_1a_4+a_3a_4)t+t^2}. \tag{A.32}$$

Substituting the expressions for a_1, a_2, a_3 and a_4 and multiplying the numerator and denominator by t^2, then yields

$$\begin{aligned}(1-x^2-y^2)^{1/2}=(1-x_0^2-y_0^2)^{1/2}\{1+[&A_1(x_0,y_0,x)+A_2(x_0,.y_0,x,y)+A_1(y_0,x_0,y)+A_2(y_0,x_0,y,x)\\&+B_1(x_0,y_0,x)+B_2(x_0,y_0,x,y)+B_1(y_0,x_0,y)+B_2(y_0,x_0,y,x)\\&+B_3(x_0,y_0,x,y)]/[C_1(x_0,y_0,x)+C_2(x_0,y_0,x,y)+C_1(y_0,x_0,y)\\&+D_1(x_0,y_0,x)+D_2(x_0,y_0,x,y)+D_1(y_0,x_0,y)+D_2(y_0,x_0,y,x)\\&+E_1(x_0,y_0,x)+E_2(x_0,y_0,x,y)+E_1(y_0,x_0,y)+E_2(y_0,x_0,y,x)+E_3(x_0,y_0,x,y)]\},\end{aligned} \tag{A.33}$$

in which

$$A_1(x_0,y_0,x)=2x_0(1-x_0^2-y_0^2)(1-2x_0^2-y_0^2)(x-x_0)^3, \tag{A.34}$$

$$A_2(x_0,y_0,x,y)=2y_0(1-x_0^2-y_0^2)(1-4x_0^2-y_0^2)(x-x_0)^2(y-y_0), \tag{A.35}$$

$$B_1(x_0,y_0,x)=2(1-3x_0^2-2y_0^2+3x_0^2y_0^2+4x_0^4+y_0^4)(x-x_0)^4, \tag{A.36}$$

$$B_2(x_0,y_0,x,y)=4x_0y_0(5x_0^2+y_0^2-1)(x-x_0)^3(y-y_0), \tag{A.37}$$

$$B_3(x_0,y_0,x,y)=2(2-5x_0^2-5y_0^2+18x_0^2y_0^2+3x_0^4+3y_0^4)(x-x_0)^2(y-y_0)^2, \tag{A.38}$$

$$C_1(x_0,y_0,x)=4(1-x_0^2-y_0^2)^2(2x_0^2+y_0^2-1)(x-x_0)^2, \tag{A.39}$$

$$C_2(x_0,y_0,x,y)=8x_0y_0(1-x_0^2-y_0^2)^2(x-x_0)(y-y_0), \tag{A.40}$$

$$D_1(x_0,y_0,x)=2x_0(1-x_0^2-y_0^2)(1-4x_0^2-y_0^2)(x-x_0)^3, \tag{A.41}$$

$$D_2(x_0,y_0,x,y)=2y_0(1-x_0^2-y_0^2)(1-4x_0^2-y_0^2)(x-x_0)^2(y-y_0), \tag{A.42}$$

$$E_1(x_0,y_0,x)=(1-y_0^2)^2(x-x_0)^4, \tag{A.43}$$

$$E_2(x_0,y_0,x,y)=4x_0y_0(1-y_0^2)(x-x_0)^3(y-y_0), \tag{A.44}$$

$$E_3(x_0,y_0,x,y)=2(1-x_0^2-y_0^2+3x_0^2y_0^2)(x-x_0)^2(y-y_0)^2. \tag{A.45}$$

Through this rational expression the limit $\{x_0, y_0\} \to \{0, 0\}$ exists and leads to the previous result obtained from a second-order Thiele approximation of g as a function of x^2 about $x^2=0$. In Fig. 17 the vertical slowness ($g=c\gamma$) as a function of horizontal slowness ($x=cp$ and $y=icq=0$) with $\mathrm{Im}\{x\}=+0$ is shown for $(x_0, y_0)=(\frac{1}{2}, 0)$.

Appendix B. Closed-form expressions for the second-order modified Cagniard contour

In this appendix, we derive closed-form expressions for the modified Cagniard contour in the second-order Thiele approximation. We assume that $r\neq 0$ so that the contour equation is cubic in p. For the solution of a cubic equation, we employ Cardano's formula [45]. The contour equation (47) is written as

$$Ap^3+Bp^2+Cp+D=0, \tag{B.1}$$

with $A\neq 0$, and the Jacobian as

$$\partial_\tau p=\frac{1-\frac{1}{4}p^2c^2}{C+2Bp+3Ap^2}, \tag{B.2}$$

with

$$A=-(1/4)c^2r, \qquad B=(1/4)c^2[\tau-3|x_3|/c], \qquad C=r[1+(1/4)c^2q^2],$$
$$D=(|x_3|/c)[1+(3/4)c^2q^2]-\tau[1+(1/4)c^2q^2].$$

The equation $\partial_p\tau=0$ (cf. eq. (51)) reduces to

$$3Ap^2+2Bp+C=0 \tag{B.3}$$

as long as the contour stays away from $p=2/c$. The solution of eq. (B.1) is written as $p(\tau, q)$, i.e., we omit the superscript II.

The discriminant associated with Cardano's formula follows from eq. (B.1) and eq. (B.3) upon elimination of p, and is given by

$$\Delta_p=G^2-H^3, \tag{B.4}$$

with

$$H=(1/9)(B^2-3AC) \tag{B.5}$$

and

$$G=(1/2)(A^2D-(1/3)ABC+(2/27)B^3). \tag{B.6}$$

Δ_p is of fourth degree in τ. First, we analyze the sign of the discriminant as a function of τ for a given q. To this end, we have to evaluate the roots of the quartic equation $\Delta_p=0$. As shown in Section 4, this equation has only two real positive solutions $\tau=T_{1,2}(q)$, which can be explicitly obtained by the method of Descartes [46]. However, in the evaluation of the space-time wave, we need the inverse relations $q=Q_{1,2}(\tau)$. Hence, we rewrite the quartic equation in τ as a cubic equation in q^2 (up to a factor $-12^{-3}16^{-1}c^6r^2$):

$$\mathscr{A}(c^2q^2)^3+\mathscr{B}(c^2q^2)^2+\mathscr{C}c^2q^2+\mathscr{D}=0, \tag{B.7}$$

and analyze the sign of the discriminant as a function of q for a given τ. The coefficients are the following functions of τ:

$$\mathscr{A}=(1/4)r^4, \qquad \mathscr{B}=-(1/2)r^2c^2\tau^2+3|x_3|r^2c\tau-(9/2)x_3^2r^2+3r^4,$$
$$\mathscr{C}=(1/4)c^4\tau^4-3|x_3|c^3\tau^3+(1/2)(27x_3^2-8r^2)c^2\tau^2-3|x_3|(9x_3^2-2r^2)c\tau+(81/4)x_3^4+18x_3^2r^2+12r^4,$$
$$\mathscr{D}=c^4\tau^4-10|x_3|c^3\tau^3+4(9x_3^2-2r^2)c^2\tau^2-6|x_3|(9x_3^2+4r^4)c\tau+27x_3^4+36x_3^2r^2+16r^4.$$

The solutions of this equation in turn can be found with Cardano's formula. To this end, we have to introduce another discriminant, Δ_q, given by

$$\Delta_q=\mathscr{G}^2-\mathscr{H}^3, \tag{B.8}$$

with

$$\mathscr{H}=(1/9)(\mathscr{B}^2-3\mathscr{A}\mathscr{C}) \tag{B.9}$$

and

$$\mathscr{G}=(1/2)(\mathscr{A}^2\mathscr{D}-(1/3)\mathscr{A}\mathscr{B}\mathscr{C}+(2/27)\mathscr{B}^3). \tag{B.10}$$

As has been shown in Section 4, $T_1(q)<T_2(q)$ for all q, and $\partial_q T_{1,2}(q)>0$ when $q>0$. Hence, when $\tau\geqslant T_2(0)$, there must be at least two real solutions for q. Then $\Delta_q<0$, and we can introduce $\{\mathscr{R}, \phi\}$ according to

$$(-\Delta_q)^{1/2}=\mathscr{R}\sin(\phi) \tag{B.11}$$

and

$$-\mathscr{G}=\mathscr{R}\cos(\phi). \tag{B.12}$$

That is,

$$\mathscr{R}=\mathscr{H}^{3/2}\geqslant 0, \qquad \phi=\arccos(-\mathscr{G}\mathscr{H}^{-3/2})\in[0,\pi]. \tag{B.13}$$

Using these expressions, we find the real positive solutions $c^2Q_{1,2}^2(\tau)$ of eq. (B.7):

$$Q_2^2(\tau)=c^{-2}\frac{1}{\mathscr{A}}\left[-\frac{\mathscr{B}}{3}+2\mathscr{R}^{1/3}\cos\left(\frac{\phi+4\pi}{3}\right)\right], \tag{B.14}$$

$$Q_1^2(\tau)=c^{-2}\frac{1}{\mathscr{A}}\left[-\frac{\mathscr{B}}{3}+2\mathscr{R}^{1/3}\cos\left(\frac{\phi}{3}\right)\right], \tag{B.15}$$

when $\tau\geqslant T_2(0)$. When $T_1(0)\leqslant\tau<T_2(0)$, we have

$$Q_1^2(\tau)=c^{-2}\frac{1}{\mathscr{A}}\left[-\frac{\mathscr{B}}{3}+2\mathscr{R}^{1/3}\cos\left(\frac{\phi}{3}\right)\right] \tag{B.16}$$

if $\Delta_1<0$, and

$$Q_1^2(\tau)=c^{-2}\frac{1}{\mathscr{A}}\left[-\frac{\mathscr{B}}{3}+[-\mathscr{G}+(\Delta_q)^{1/2}]^{1/3}+[-\mathscr{G}-(\Delta_q)^{1/2}]^{1/3}\right] \tag{B.17}$$

if $\Delta_q\geqslant 0$, taking real cubic roots; $Q_2(\tau)$ fails to be real in this case. We take positive real square roots to obtain $Q_{1,2}(\tau)$. By analyzing the sign of the discriminant of the contour solution, we find that $\Delta_p>0$ when $T_1(q)<\tau<T_2(q)$.

We restrict ourselves to contours with $\mathrm{Re}\{p\} \geqslant 0$. When $T_1(q) < \tau < T_2(q)$, $\Delta_p > 0$ and we get

$$p(\tau, q) = \frac{1}{A}\left[-\frac{B}{3} + uw^* + vw\right], \tag{B.18}$$

as well as its complex conjugate $p^*(\tau, q)$. Here,

$$u = [-G + \Delta_p^{1/2}]^{1/3} \tag{B.19}$$

and

$$v = [-G - \Delta_p^{1/2}]^{1/3}, \tag{B.20}$$

whereas $w = \exp(\frac{3}{2}\pi\mathrm{i})$ is the primitive cubic root of 1. In eqs. (B.19) and (B.20) we take the real roots.

The shape of the wave front follows from eq. (B.7) upon substituting $q = 0$. The resulting equation, $\mathscr{D} = 0$, is written as

$$16r^4 + \mathscr{F}r^2 + \mathscr{K} = 0. \tag{B.21}$$

At a "snapshot" time τ the solutions are given by

$$r_1(x_3) = \left[-\frac{1}{32}(\mathscr{F} - \Delta_r^{1/2})\right]^{1/2} \tag{B.22}$$

for the fast wave, and

$$r_2(x_3) = \left[-\frac{1}{32}(\mathscr{F} + \Delta_r^{1/2})\right]^{1/2} \tag{B.23}$$

for the slow wave. Here,

$$\mathscr{F} = -4[2c^2\tau^2 + 6|x_3|c\tau - 9x_3^2], \tag{B.24}$$

whereas the discriminant, Δ_r, is given by

$$\Delta_r = \mathscr{F}^2 - 64\mathscr{K} = -16x_3^4\left[3 - 4\frac{c\tau}{|x_3|}\right]^3, \tag{B.25}$$

in which

$$\mathscr{K} = (c\tau - |x_3|)(c\tau - 3|x_3|)^3. \tag{B.26}$$

The discriminant is always positive when $\tau \geqslant |x_3|/c$. This is the minimum arrival time of the fast wave occurring at $r = 0$. The slow wave front contains cusps at $r = 0$, $|x_3| = c\tau/3$. The fast wave front contains cusps at $r = c\tau/2$, $x_3 = 0$. The different wave fronts are shown in Figs. 18 and 19. They show similarities with the wave front of a hyperbolic differential equation of a different nature considered by Courant and Hilbert [47, pages 588–589].